LU TP 02–46
hep-ph/0212264
December 2002

Baryon Number Violation and String Topologies

T. Sjöstrand[1] and P. Z. Skands[2]

Department of Theoretical Physics,
Lund University,
Sölvegatan 14A,
S-223 62 Lund, Sweden

Abstract

In supersymmetric scenarios with broken R-parity, baryon number violating sparticle decays become possible. In order to search for such decays, a good understanding of expected event properties is essential. We here develop a complete framework that allows detailed studies. Special attention is given to the hadronization phase, wherein the baryon number violating vertex is associated with the appearance of a junction in the colour confinement field. This allows us to tell where to look for the extra (anti)baryon directly associated with the baryon number violating decay.

[1]torbjorn@thep.lu.se
[2]zeiler@thep.lu.se

1 Introduction

There are good reasons to consider supersymmetry (SUSY) as the next logical step in formulating a consistent theory of particle physics. It complements the Standard Model by the possibility to secure the Higgs potential against excessive radiative corrections, and provides a framework for understanding electroweak symmetry breaking. SUSY is the largest symmetry, within the requirements of conventional field theory, where internal symmetry groups can be combined with the space–time Poincaré group. It thereby points the way towards a unified theory also including gravity, e.g. based on superstrings. For this and other reasons SUSY has been a prime scenario in the search for manifestations of physics beyond the Standard Model. Furthermore, in planning future experiments, SUSY offers a broad range of distinctive signatures that form convenient targets for detector performance and analysis strategies.

In the Minimal Supersymmetric extension of the Standard Model (MSSM), the standard particle content, extended to two Higgs doublets, is doubled up by the presence of superpartners to all normal particles. A multiplicative quantum number called R-parity may be defined by $R = (-1)^{2S+3B+L}$, where S is the particle spin, B its baryon number and L its lepton number, such that normal particles have $R = 1$ while the superpartners have $R = -1$. If R-parity is conserved, supersymmetric particles are pair produced, and the Lightest Supersymmetric Particle (LSP) is stable and hence a Dark Matter candidate. However, there is at present no deep theoretical motivation why R-parity should not be broken. This paves the way both for baryon number violating (BNV = baryon number violation/violating in the following) and lepton number violating (LNV) processes. If both of these are allowed, proton decay would be extremely rapid, unless the relevant couplings are abnormally tiny [1]. As a rule, phenomenology is therefore based on assuming either BNV or LNV, but not both.

The supersymmetric particles that could be produced in high-energy colliders normally are not directly observable: either they decay rapidly or they are weakly interacting and escape detection. With R-parity conserved, the signals would consist of jets, leptons and missing $E_\perp$ from escaping neutrinos and LSP's. In scenarios with BNV the main decay product is jets, with only few leptons or neutrinos, and so observability above QCD backgrounds becomes far from trivial at hadron colliders such as the Tevatron or the LHC. In order to carry out realistic studies it is therefore necessary to have a detailed understanding of the properties of both signal and background events. The prime tool for achieving such an understanding is to implement the relevant processes in event generators, where simulated events can be studied with all the analysis methods that could be used on real events. Main generators used for SUSY studies include Isajet [2], Herwig [3], Susygen [4], and Pythia [5]. Traditionally the Pythia framework assumes R-parity conservation, but recently LNV processes have been implemented and some first studies carried out [6, 7].

In the past, BNV has been modelled [8, 9] and studied [10] in detail in the Herwig framework, with emphasis on the perturbative aspects of the production process. In this article we present a corresponding implementation in Pythia where a special effort is dedicated to the non-perturbative aspects, i.e. what happens with the (anti)baryon number generated by the BNV. This allows us to address the possibility to obtain the "smoking-gun" evidence that a BNV decay has occurred, with questions such as *Could the presence of a violated baryon number be directly observed?* and *If so, what strategy should be used?*. A brief presentation of this work can be found in [11].

In addition, many differences exist between the Pythia and Herwig physics scenar-

ios, for parton showers and underlying events, allowing useful cross-checks to be carried out and uncertainties to be estimated.

The outline of the article is as follows. In section 2, we briefly summarize the short distance physics associated with BNV SUSY and give an account of its implementation into PYTHIA. Next, in section 3, we turn our attention to a parton-shower description of gluon emission in BNV decays. In section 4, the special aspects related to the presence of a net baryon number in the hadronization process are described and an approach based on the Lund model of QCD strings is developed. In section 5 we concentrate on tests of the model, with special attention to the fate of the (anti)baryon produced by BNV. Some (semi)realistic studies are collected in section 6. Finally, section 7 summarizes and gives an outlook.

2 The Baryon Number Violation Scenario

In Supersymmetric theories, it is usually convenient to work at the superpotential level rather than at the Lagrangian level, since the former has a simpler structure and is in any case related to the latter by straightforward manipulations, see e.g. [12]. The most general superpotential which can be written down for the MSSM includes 4 R-parity odd terms:

$$W_{\mathrm{RPV}}^{\mathrm{MSSM}} = \frac{1}{2}\lambda_{ijk}\epsilon^{ab}L_a^i L_b^j \bar{E}^k + \lambda'_{ijk}\epsilon^{ab}L_a^i Q_b^{j\alpha}\bar{D}_\alpha^k + \frac{1}{2}\lambda''_{ijk}\epsilon^{\alpha_1\alpha_2\alpha_3}\bar{U}_{\alpha_1}^i \bar{D}_{\alpha_2}^j \bar{D}_{\alpha_3}^k + \kappa_i L_a^i H_2^a \quad (1)$$

where i, j, k run over generations, a, b are $\mathrm{SU}(2)_L$ isospin indices, and $\alpha_{(i)}$ runs over colours. L and Q are the SU(2) doublet (left-handed) chiral superfields for (s)leptons and (s)quarks, respectively, and E, U, and D are the SU(2) singlet (right-handed) superfields for charged (s)leptons, (s)up type, and (s)down type quarks, respectively. The last term represents a mixing between the left-handed (s)leptons and one of the Higgs superfields.

There are two noteworthy aspects about the third term in eq. (1), which we shall henceforth refer to as the "UDD" term: 1) it is the only one which has a non-zero baryon number (all the others violate lepton number), and 2) the colour indices have a Levi-Civita tensor structure. Of course, these two aspects are really one and the same. They express the simple fact that, since SU(3) of colour is unbroken, the only way to make a colour singlet is to combine the three colours antisymmetrically, e.g. as used in constructing ordinary baryon wavefunctions.

In a B-conserving theory like the SM or the R-conserving MSSM, there is no colour antisymmetric perturbative interaction term, i.e. no term with a colour structure like that of the UDD term. Apart from extreme occurrences, like knocking two valence quarks out of the same proton in different directions, by two simultaneous but separate interactions, normal high-energy events would therefore not fully display the antisymmetric colour structure of the proton. Instead, it is normally enough to consider a baryon as consisting of a colour triplet quark and a colour antitriplet diquark, where the internal structure of the latter need not be specified. So what is different about the UDD term is that it allows the production of three colour carriers at large momentum separation, without the creation of corresponding anticolour carriers. It is the necessary SU(3) gauge connection between these three partons that will lead us in the development of the nonperturbative framework.

A further point about the UDD term is that the contraction of the ϵ tensor with $\bar{D}^j\bar{D}^k$ implies that λ''_{ijk} should be chosen antisymmetric in its last two indices, since a (j,k)-symmetric part would cancel out.

The part of the Lagrangian coming from the UDD superpotential term in which we are interested is:

$$\mathcal{L}_{\rm BNV} = \tfrac{1}{2}\lambda''_{ijk}\epsilon^{\alpha_1\alpha_2\alpha_3}\left(\bar{u}^i_{R\alpha_1}(\tilde{\rm d}^*)^j_{R\alpha_2}({\rm d}^c)^k_{R\alpha_3} + \bar{\rm d}^j_{R\alpha_1}(\tilde{\rm u}^*)^i_{R\alpha_2}({\rm d}^c)^k_{R\alpha_3} - (j \leftrightarrow k)\right) + h.c. \quad (2)$$

where we have made the choice of not yet using any of the antisymmetry requirements, so that the ordinary Einstein summation convention applies. Superscript c implies charge conjugation and $\tilde{\rm q}^*$ denotes a charge (=complex) conjugate squark. From this, the possible lowest-order BNV 3-point functions can immediately be read off. In this paper, we only consider sparticle decays; BNV production mechanisms are ignored. This is first and foremost a conservative approach, since any additional sparticle production could only increase the observable signal. Secondly, the underestimation of the sparticle production cross sections is small as long as 1) the BNV couplings are small compared to the gauge couplings and 2) the squarks are not so heavy that single-squark production via BNV is significantly enhanced over the ordinary pair production processes. For discussions of single squark production, see [13].

Combining the vertices in eq. (2) with the full MSSM Lagrangian, also decays involving one or more gauge couplings are clearly possible, e.g. neutralino decay via $\tilde{\chi}^0 \to \tilde{\rm q}_i(\to \bar{\rm q}_j\bar{\rm q}_k)\bar{\rm q}_i$. The BNV SUSY decay processes currently implemented in Pythia, with Born level matrix elements as calculated by [8], are:

1)	$\tilde{\rm d}_{jn}$	$\to$	$\bar{\rm u}_i\bar{\rm d}_k$	(36)
2)	$\tilde{\rm u}_{in}$	$\to$	$\bar{\rm d}_j\bar{\rm d}_k$	(18)
3)	$\tilde{\chi}^0_n$	$\to$	${\rm u}_i{\rm d}_j{\rm d}_k$	(144)
4)	$\tilde{\chi}^+_n$	$\to$	${\rm u}_i{\rm u}_j{\rm d}_k$	(30)
5)	$\tilde{\chi}^+_n$	$\to$	$\bar{\rm d}_i\bar{\rm d}_j\bar{\rm d}_k$	(14)
6)	$\tilde{\rm g}$	$\to$	${\rm u}_i{\rm d}_j{\rm d}_k$	(36)

where n runs over the relevant mass eigenstates: $n \in \{L, R\}$ for the first two generations of squarks, $n \in \{1, 2\}$ for the third generation squarks and the charginos, and $n \in \{1, ..., 4\}$ for the neutralinos. The numbers in brackets are the number of modes when summed over n, i, j, and k, and over charge conjugate modes for the Majorana particles.

The matrix elements for these processes, as implemented in Pythia, are not quite identical to those used in Herwig. Most importantly, Pythia uses running masses and couplings at some points where Herwig does not. See [7] for a list of these differences.

When calculating the partial widths (and hence also the rates) into these channels, we integrate the matrix elements over the full phase space with massive b and t quarks, and massive sparticles. All other particles are only treated as massive when checking whether the decay is kinematically allowed or not, i.e. they are massless in the phase space integration.

A feature common to both programs is how double-counting in the BNV three-body modes is avoided. The diagrams for these modes contain intermediate squarks which may be either on or off the mass shell, depending on the other masses involved in the process. If a resonance can be on shell, we risk doing double counting since Pythia is then already allowing the process, in the guise of two sequential $1 \to 2$ splittings. Technically, this means that the list of $1 \to 3$ BNV widths obtained by a call to `PYSTAT(2)` only represent the non-resonant contributions, the resonant ones being accounted for by sequences of $1 \to 2$ splittings in other parts of the code.

In the description of the momentum distribution in a three-body resonance decay, the default Pythia procedure is to assume an isotropic phase space, i.e. the matrix-element

information used above to obtain partial widths is neglected here. This should not be a bad approximation when the intermediate squark propagators are far from mass shell over the full phase space and therefore do not vary much, but could be a problem when a squark mass (plus the mass of the corresponding quark) is only slightly above the gaugino one. In section 5 we return to this issue, comparing with HERWIG, where the full, unintegrated matrix elements are used to give a more correct phase space population.

3 Parton Showers

The production and decay of unstable particles is normally associated with bremsstrahlung emission of gluons and/or photons as applicable. This radiation is conveniently described in the parton-shower language, where the effects of multiple emissions are explicitly included by iterative applications of the relevant splitting kernels, such as $q \to qg$, $g \to gg$, $g \to q\overline{q}$ and $q \to q\gamma$. Even though existing showering algorithms typically only fully resum the leading logarithms, most of the effects of next-to-leading logs are also included in the form of energy–momentum conservation, recoil effects, scale choice in α_s, coherence effects, and matching of energetic emissions to higher-order matrix elements. At LEP the PYTHIA, HERWIG and ARIADNE [14] radiation routines have been well tested. All three are found to describe the data well, although some problems exist [15]. Since ARIADNE has not been used for SUSY studies, we restrict the continued discussion to the former two.

The HERWIG algorithm is based on an evolution variable that ensures angular ordering; subsequent emissions occur at smaller and smaller angles. Thereby coherence effects are respected, i.e. double-counting of emission is avoided. The colour flow of the hard process defines cones around the partons, within which all emissions occur. In the limit where each emitted gluon is much softer than the hard-scattering partons, and much softer than all preceding gluons emitted, this approach can be shown to give the correct emission rate, and also when going away from this limit it should provide a good overall description. However, a consequence of the way the kinematics of the algorithm is constructed is that "dead zones" occur, within which no emission at all is possible [16]. Thus, in $e^+e^- \to q\overline{q}g$ events, the region of energetic gluon emission at large angles to both the q and $\overline{q}$ is completely empty. The solution [16] is to combine two classes of events, both $q\overline{q}$ and $q\overline{q}g$ ones, with the latter picked in the "dead zone" region of the three-body phase space according to the relevant matrix elements. All events, i.e. from either class, are then allowed to shower further. However, such corrections have only been worked out for a few cases, e.g. $e^+e^- \to q\overline{q}g$ and top decay [17].

The PYTHIA algorithm is based on evolution in the virtuality of the emitting parton, with the requirement of angular ordering enforced by vetoing non-angular-ordered emissions. This gives a less exact description of coherence in the soft-gluon limit. Yet it does allow the full three-body phase space to be populated, simply by not imposing any angular ordering constraint for the first emission of each of the two original partons. As it turns out, the incoherent addition of radiation from these two sources tends to give an overestimation of the $q\overline{q}g$ rate in the hard, non-collinear gluon region, while the soft and collinear regions give what they should. It is therefore straightforward to introduce a correction factor, whereby a fraction of the emissions are vetoed, so that the remaining fraction agrees with the desired three-jet rate [18]. Some years ago, the relevant gluon-emission corrections were calculated and implemented for most two-body decays within the SM and the MSSM, with R-parity conserved [19].

Normal processes are characterized by unbroken colour lines: the colours present in the initial state will also be there in the final state, with the proviso that opposite colours and anticolours may be pair-produced or annihilated. This information is used in parton showers, e.g. to set up emission cones. BNV processes are different in this respect: in a $\tilde{q} \to \overline{qq}$ branching a blue colour line may end and antired and antigreen begin. Therefore the standard rules need to be supplemented. In HERWIG an effort has been made to study the different new topologies and use the soft-gluon eikonal, i.e. spin-independent, expressions to set up the relevant maximum emission cones in the different processes [8]. Still, the "dead zone" issue is not addressed, meaning that the rate of energetic, wide-angle gluon emission is almost certainly underestimated.

By contrast, we shall here allow emission over the full phase space, like before. However, not having calculated the corresponding matrix-element correction factors, one should not expect the correct rate in the hard-gluon region. Technically, in the lack of further knowledge, the $\tilde{q} \to \overline{qq}$ process is corrected to the eikonal answer for a colour singlet decaying to a triplet plus an antitriplet [19]. For three-body decays such as $\tilde{\chi} \to qqq$ or $\tilde{g} \to qqq$, no matrix element corrections are available.

With three (or more) primary partons to shower, one is left with the issue how the kinematics from the on-shell matrix elements should be reinterpreted for an off-shell multiparton configuration. We have made the arbitrary choice of preserving the direction of motion of each parton in the rest frame of the system, which means that all three-momenta are scaled down by the same amount, and that some particles gain energy at the expense of others. Mass multiplets outside the allowed phase space are rejected and the evolution continued.

In principle, radiation in the initial and final states may interfere, thereby requiring the inclusion of further coherence conditions. The extent of such interference critically depends on the width of the intermediate resonance: only gluons with energies below this width are emitted coherently from initial and final partons [20]. We here assume that the resonances are sufficiently narrow that such interference effects can be neglected; see further the discussion in section 4.5.

The bottom line is that PYTHIA likely overestimates the hard-gluon emission rate, whereas HERWIG underestimates it. This makes it interesting to compare the two descriptions, and possibly to use differences as a first estimation of systematic uncertainties in our current description of BNV processes.

4 String Topologies

Up till now we have considered short-distance processes, where perturbation theory provides a valid description in terms of quarks, gluons and other fundamental particles. At longer distances, the running of the strong coupling α_s leads to confinement and a breakdown of the perturbative description of QCD processes. Instead there is a transition to a nonperturbative régime, characterized by hadrons rather than by partons. In the lack of an exact approach, this hadronization process must be modelled. The perhaps most successful and frequently used approach is the Lund string fragmentation model [21].

This approach has not before been applied to the colour topologies encountered in BNV. We therefore here extend the string model by the introduction of a junction, where three string pieces come together. Effectively, it is this junction that carries the (anti)baryon number that is generated by a BNV process. The hadronization in the region around the junction will therefore be of special interest.

4.1 The normal string

In this subsection we summarize some properties of the ordinary Lund string model, highlighting the concepts that will be needed for the developments in the remainder of the article. Readers who are already familiar with the fundamentals of the string model may wish to proceed directly to the next subsection.

To illustrate the string model, it is useful to start with the simplest possible system, a colour-singlet $\mathrm{q\overline{q}}$ 2-jet event, as produced in $\mathrm{e^+e^-}$ annihilation. Here lattice QCD studies lend support to a linear confinement picture in the absence of dynamical quarks, i.e. in the quenched approximation [22]. Thus the energy stored in the colour dipole field between a charge and an anticharge increases linearly with the separation between the charges, if the short-distance Coulomb term is neglected. This is quite different from the behaviour in QED, and is related to the non-Abelian character of QCD. The dynamical mechanisms involved are not fully understood, however.

The assumption of linear confinement provides the starting point for the string model. As the q and $\overline{\mathrm{q}}$ partons move apart from their common production vertex, the physical picture is that of a colour vortex line, or maybe a colour flux tube, being stretched between the q and the $\overline{\mathrm{q}}$. (The difference between these two terminologies is related to whether the QCD vacuum more resembles a type II or a type I superconductor. This is an interesting question by itself, with the vortex line analogy somewhat favoured by theoretical prejudice, but it will not be crucial for the continued discussion here.) The transverse dimensions of the tube are of typical hadronic sizes, roughly 1 fm. If the tube is assumed to be uniform along its length, this automatically leads to a confinement picture with a linearly rising potential. In order to obtain a Lorentz covariant and causal description of the energy flow due to this linear confinement, the most straightforward approach is to use the dynamics of the massless relativistic string with no transverse degrees of freedom. The mathematical, one-dimensional string can be thought of as parameterizing the position of the axis of a cylindrically symmetric flux tube or vortex line. From hadron spectroscopy, the string constant, i.e. the amount of energy per unit length, is deduced to be $\kappa \approx 1$ GeV/fm.

For a massless $\mathrm{q\overline{q}}$ pair moving out along the $\pm z$ axis, the original energy and momentum of the quark is then reduced with time according to

$$E_{\mathrm{q}}(t) = p_{z\mathrm{q}}(t) = E_{\mathrm{q}}(0) - \kappa t \ , \tag{3}$$

with a corresponding equation for $E_{\overline{\mathrm{q}}}(t) = -p_{z\overline{\mathrm{q}}}(t)$. This classical equation of motion obviously does not take into account the quantum mechanical uncertainty relation; in this sense one may conceive of the (unmeasured) space–time picture as a subordinated intermediate step in the derivation of the (measured) energy–momentum picture.

If the quark instead has a nonvanishing rest mass m_{q} the equation of motion is

$$\frac{\mathrm{d}p_{z\mathrm{q}}(t)}{\mathrm{d}t} = \frac{\mathrm{d}p_{z\mathrm{q}}(t)}{\mathrm{d}E_{\mathrm{q}}(t)} \frac{\mathrm{d}E_{\mathrm{q}}(t)}{\mathrm{d}t} = \frac{E_{\mathrm{q}}(t)}{p_{z\mathrm{q}}(t)} \left(-\kappa \frac{\mathrm{d}z}{\mathrm{d}t} \right) = \frac{E_{\mathrm{q}}(t)}{p_{z\mathrm{q}}(t)} \left(-\kappa \frac{p_{z\mathrm{q}}(t)}{E_{\mathrm{q}}(t)} \right) = -\kappa \ , \tag{4}$$

which has the solution

$$p_{z\mathrm{q}}(t) = p_{z\mathrm{q}}(0) - \kappa t \ ; \tag{5}$$

$$E_{\mathrm{q}}(t) = \sqrt{E_{\mathrm{q}}^2(0) - 2\kappa t\, p_{z\mathrm{q}}(0) + \kappa^2 t^2} \ . \tag{6}$$

A key aspect, which we will make use of for the junction phenomenology below, is that the momentum loss per unit of time is independent of the quark mass.

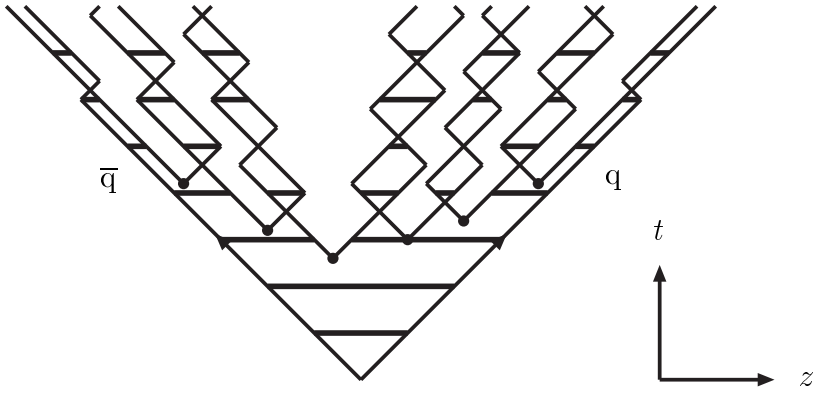

Figure 1: The breakup of an original $\mathrm{q}\overline{\mathrm{q}}$ system into a set of mesons, each represented by a yo-yo state. For simplicity quarks are here assumed massless, and so move along lightcones. The broken horizontal lines illustrate the string pieces at a few discrete times.

In the back-to-back configuration the string does not carry any net momentum, but acquires energy proportional to its total length as the q and $\overline{\mathrm{q}}$ move apart. Once the endpoint quarks have lost their momenta, they will be pulled back by the string tension and re-acquire momenta in the opposite direction, at the same time as the string length shrinks back. When the quarks meet again the force flips sign and a second half-period of the oscillation begins.

Such stable "yo-yo" modes are used as simple representations of mesons. For a high-invariant-mass $\mathrm{q}\overline{\mathrm{q}}$ system, the fragmentation into lower-mass mesons proceeds through the production of new $\mathrm{q}'\overline{\mathrm{q}}'$ pairs, corresponding to dynamical quarks in lattice QCD. Thereby the original system first splits into two colour-singlet systems, $\mathrm{q}\overline{\mathrm{q}}'$ and $\mathrm{q}'\overline{\mathrm{q}}$. If the invariant mass of either of these string pieces is large enough, further breaks occur. In the Lund model, the string break-up process is assumed to proceed until only on-mass-shell hadrons remain, each hadron corresponding to a small piece of string with a quark in one end and an antiquark in the other. This process is illustrated in Fig. 1.

In general, the different string breaks are causally disconnected. This means that it is possible to describe the breaks in any convenient order, e.g. from the quark end inwards. One therefore is led to formulate an iterative scheme for the fragmentation, as follows. Assume, as above, an initial quark q moving out along the $+z$ axis, with the antiquark going out in the opposite direction. By the production of a $\mathrm{q}_1\overline{\mathrm{q}}_1$ pair, a meson with flavour content $\mathrm{q}\overline{\mathrm{q}}_1$ is produced, leaving behind an unpaired quark q_1. A second pair $\mathrm{q}_2\overline{\mathrm{q}}_2$ may now be produced, to give a new meson with flavours $\mathrm{q}_1\overline{\mathrm{q}}_2$, etc. At each step the produced hadron takes some fraction of the available energy and momentum. This process may be iterated until all energy is used up, with some modifications close to the $\overline{\mathrm{q}}$ end of the string in order to make total energy and momentum come out right, since all hadrons are required to be on mass shell.

The choice of starting the fragmentation from the quark end is arbitrary, however. A fragmentation process described in terms of starting at the $\overline{\mathrm{q}}$ end of the system and fragmenting towards the q end should be equivalent. This "left–right" symmetry constrains the allowed shape of the fragmentation function $f(z)$, where z is the fraction of the remaining light-cone momentum $E \pm p_z$ (+ for the q jet, − for the $\overline{\mathrm{q}}$ one) taken by each new particle. The resulting "Lund symmetric fragmentation function" has two main

free parameters, which are determined from data.

Viewed in time, the fragmentation process actually starts near the middle of the event and spreads outwards. The $\mathrm{q}'\overline{\mathrm{q}}'$ production vertices on the average occur along a hyperbola of constant invariant time τ, $\tau^2 = t^2 - z^2$, so even if the string is boosted along the z axis it is still the slow particles in this new frame that are the ones produced first. In this sense, a Lorentz-covariant "inside-out" cascade can technically be described by an "outside-in" iteration scheme. As an order-of-magnitude, $\langle\tau\rangle \approx 1.5$ fm or $\langle\kappa\tau\rangle \approx 1.5$ GeV.

In order to generate the quark–antiquark pairs $\mathrm{q}'\overline{\mathrm{q}}'$ which lead to string break-ups, the Lund model invokes the idea of quantum mechanical tunnelling. This gives a flavour-independent Gaussian spectrum for the $p_\perp$ of $\mathrm{q}'\overline{\mathrm{q}}'$ pairs. Since the string is assumed to have no transverse excitations, this $p_\perp$ is locally compensated between the quark and the antiquark of the pair. The total $p_\perp$ of a hadron is made up out of the $p_\perp$ contributions from the quark and antiquark that together form the hadron. Some contribution of soft unresolved perturbative gluon emission may also effectively be included in this description.

The tunnelling picture implies a suppression of heavy-quark production, $\mathrm{u} : \mathrm{d} : \mathrm{s} : \mathrm{c} \approx 1 : 1 : 0.3 : 10^{-11}$. Charm and heavier quarks hence are not expected to be produced in the soft fragmentation, but only in perturbative parton-shower branchings $\mathrm{g} \to \mathrm{q}\overline{\mathrm{q}}$.

When the quark and antiquark from two adjacent string breaks are combined to form a meson, it is necessary to invoke an algorithm to choose between the different allowed possibilities, notably between pseudoscalar and vector mesons. Here the string model is not particularly predictive. Qualitatively one expects a 1 : 3 ratio, from counting the number of spin states, multiplied by some wave-function normalization factor, which should disfavour heavier states.

A tunnelling mechanism can also be used to explain the production of baryons. In the simplest possible approach, a diquark in a colour antitriplet state is just treated like an ordinary antiquark, such that a string can break either by quark–antiquark or antidiquark–diquark pair production [23]. A more complex scenario is the "popcorn" one [24], where diquarks as such do not exist, but rather quark–antiquark pairs are produced one after the other. This latter picture gives a less strong correlation in flavour and momentum space between the baryon and the antibaryon of a pair.

In all fairness, it should be said that the description of baryon production is one of the less predictive aspects of the Lund model, with many free parameters for the flavour composition that need to be determined from the data. Most single-baryon spectra are well described after such a tuning, except possibly at very large momentum fractions [25]. A reasonable description is also obtained for baryon–antibaryon correlations, although with some disagreements. For the aspects that we will study here, and within the precision allowed by other considerations, the baryon production model should be fully adequate, however.

If several partons are moving apart from a common origin, the details of the string drawing become more complicated. For a $\mathrm{q}\overline{\mathrm{q}}\mathrm{g}$ event, a string is stretched from the q end via the g to the $\overline{\mathrm{q}}$ end, Fig. 2, i.e. the gluon is a kink on the string, carrying energy and momentum. As a consequence, the gluon has two string pieces attached, and the ratio of gluon to quark string force is 2, a number which can be compared with the ratio of colour-charge Casimir operators, $N_C/C_F = 2/(1 - 1/N_C^2) = 9/4$. In this, as in other respects, the string model can be viewed as a variant of QCD where the number of colours N_C is not 3 but infinite. Note that the factor 2 above is independent of the actual kinematical configuration: a smaller opening angle between two partons corresponds to a smaller string length being drawn out per unit time, but also to a larger transverse velocity of the string piece, thereby increasing its energy density. In fact, these two factors exactly

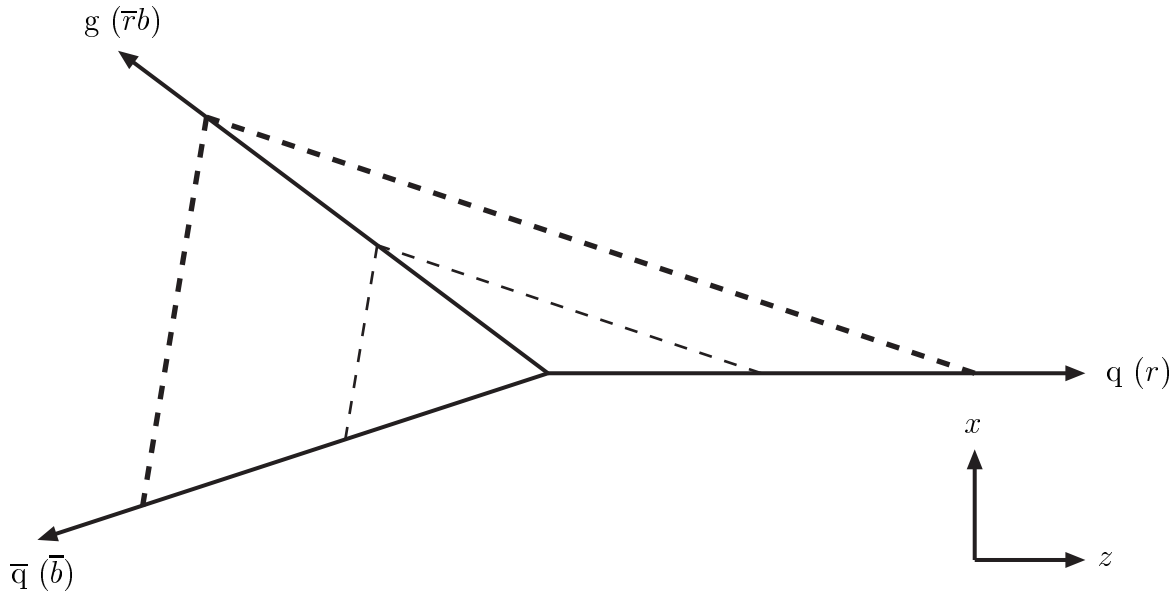

Figure 2: The string motion in a q$\overline{\mathrm{q}}$g system, neglecting hadronization. The q, $\overline{\mathrm{q}}$ and g move out from the common origin, all with the speed of light and along straight lines, in the limit that quark masses are neglected. The connecting dashed lines illustrate the string pieces at two times. A possible colour assignment is indicated within brackets.

cancel so that the energy loss per unit time indeed becomes the same.

The q$\overline{\mathrm{q}}$g string will fragment along its length. To first approximation this means that there is one fragmenting string piece between q and g and a second one between g and $\overline{\mathrm{q}}$. One hadron is straddling both string pieces, i.e. sitting around the gluon corner. The rest of the particles are produced as in two simple q$\overline{\mathrm{q}}$ strings, but strings boosted with respect to the overall CM frame. When considered in detail, the string motion and fragmentation is more complicated, with the appearance of additional string regions during the time evolution of the system [26]. These corrections are especially important for soft and collinear gluons, since they provide a smooth transition between events where such radiation took place and events where it did not. Therefore the string fragmentation scheme is "infrared safe" with respect to soft or collinear gluon emission.

4.2 The junction

As we saw above, meson states can be represented by little yo-yo's, with a string piece stretched between the q and $\overline{\mathrm{q}}$. What would be the corresponding representation for a baryon? In normal string fragmentation the issue is not so interesting, since the hadron size is consistent with the string width, meaning the internal structure is not really resolved. Thus the mesonic yo-yo is more of a convenient concept for book-keeping, and it is only for higher-mass systems that the elongated string structure really becomes of relevance. The equivalent situation for a baryon state would then be when several valence quarks are kicked out of an incoming proton or, as here, when baryon number is violated in Supersymmetry. In its simplest form, it can be illustrated by the decay $\tilde{\chi}_1^0 \to \mathrm{u}_i\mathrm{d}_j\mathrm{d}_k$, or equivalently a proton in which all valence quarks are kicked out in different directions at the same time.

Our solution here is to introduce the concept of a junction, in which a string piece from

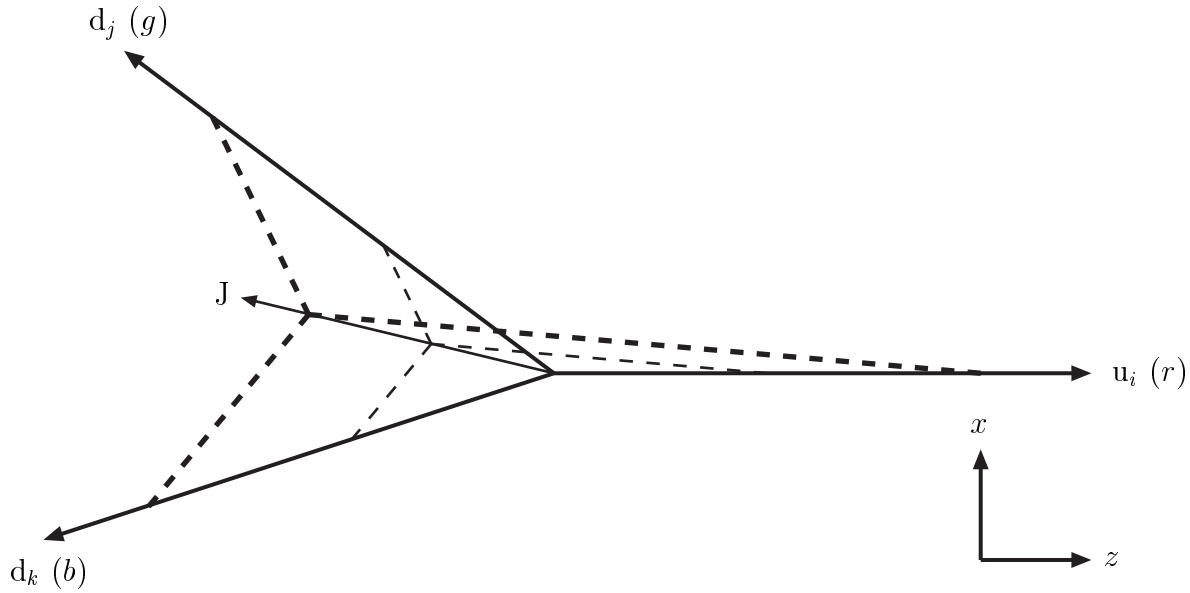

Figure 3: The string motion in a junction system, neglecting hadronization. The u_i, d_j and d_k move out from the common origin, all with the speed of light and along straight lines, in the limit that quark masses are neglected. The thin arrow indicates the resulting motion of the junction J. The connecting dashed lines illustrate the Y-shaped string topology at two discrete times. A possible colour assignment is indicated within brackets.

each of the three quarks meet, i.e. a Y-shaped topology, Fig. 3. Each of the three strings are of the normal kind already encountered. For instance, the string from the blue d_k quark acts as if there were an antiblue antiquark in the junction position. Recall that the colours of the two other quarks add like $g + r = \overline{b}$, given that the colour representation of the quarks is totally antisymmetric so as to make the state a colour singlet. Correspondingly for the other two string pieces. Only in the immediate neighbourhood of the junction would the field topology be more complicated.

In the hadronization, ordinary $\mathrm{q}'\overline{\mathrm{q}}'$ pair production will break up each of the three string pieces. This leads to meson production, and in diquark/popcorn scenarios also to baryon–antibaryon pair production, but not to the production of any net baryon number. Instead it is the three q$'$s nearest to the junction, one from each string piece, that team up to form the baryon that is associated with the original baryon number, Fig. 4. In this sense the junction, by its colour topology, becomes the carrier of the baryon number of the system, rather than the three original quarks. This baryon typically comes to have a small momentum in the rest frame of the junction, as we shall see. This holds also in the rest frame of a typical $\tilde{\chi}_1^0 \to \mathrm{u}_i\mathrm{d}_j\mathrm{d}_k$ decay, where the three quarks move out in widely separated directions, since the junction then has a small velocity.

The concept of a junction is not new. It was introduced in the early string model of hadrons [27, 28, 29], and has been used in confinement studies to set up the colour structure of baryons in the same way as we do here [30]. Indeed, the simplest locally gauge invariant operator of baryon number unity that can be constructed in SU(3) is [29]:

$$B_{i_1 i_2 i_3} = \epsilon^{\alpha_1\alpha_2\alpha_3} \prod_{n=1}^{3} P\Big[e^{ig\int_{\mathcal{P}(x,x_n)} A_\mu \mathrm{d}x^\mu} q_{i_n}(x_n)\Big]_{\alpha_n} \tag{7}$$

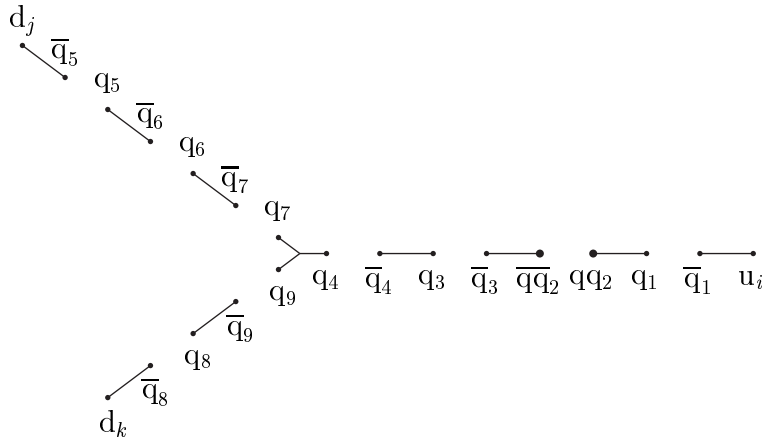

Figure 4: Hadronization by $q'\overline{q}'$ production in a junction string topology. The figure is in an abstract "flavour space", to be related to a space–time topology like Fig. 3, with flavours belonging to the same hadron connected by string pieces. The labelling of new quarks is arbitrary. The $q_4q_7q_9$ hadron carries the original baryon number, while q_1qq_2 and $\overline{qq}_2\overline{q}_3$ correspond to the possibility of baryon–antibaryon pair production in the hadronization process, and the rest represents normal meson production.

where i_n and α_i are indices for flavour and colour, respectively, A_μ is the gluon field, and P expresses ordering along the path $\mathcal{P}$ from x to x_n. Physically, this operator represents three quarks sitting at x_1, x_2, and x_3, respectively, each connected via the gluon field to the point x, which we may identify as corresponding to the locus of the string junction. Thus, from this point of view, QCD does appear to select the junction topology.

The junction concept has also been applied to the understanding of the fragmentation function of baryons in low-$p_\perp$ hadronic collisions [31], providing a more sophisticated variant of the popcorn mechanism whereby the two quarks of a diquark need not end up in the same hadron. Multiple perturbative parton–parton interactions have been suggested as a mechanism to activate the junction in proton beams [32]. And junctions have been proposed for $q\overline{q}g$ configurations, in scenarios where a separate kind of colour octet gluon string exists (which requires a string tension less than twice that of the normal colour triplet string, or else it would be energetically unfavourable) [33].

A simplified and unofficial implementation of junctions has existed in PYTHIA since many years, and been used e.g. from SUSYGEN. To the best of our knowledge, however, what we present here is the first complete scenario for the hadronization of generic junction topologies in high-energy interactions.

It could have been interesting to contrast the junction concept with some alternatives, but we have been unable to conceive of any realistic such, at least within a stringlike scenario of confinement. The closest we come is a V-shape topology, with two string pieces, similar to the $q\overline{q}g$ topology in Fig. 2. This would be obtained if one e.g. imagined splitting the colour of the upper left quark in Fig. 3 as $g = \overline{r}\overline{b}$. In such a scenario the baryon would be produced around this quark, and could be quite high-momentum. Of course, such a procedure is arbitrary, since one could equally well pick either of the three quarks to be in the privileged position of producing the key baryon. Further, with two string pieces now being pulled out from one of the quarks, the net energy stored in the string at a given (early) time is larger than in the junction case, meaning the Y junction

is energetically favoured over the V topology. For these reasons, the V scenario has not been pursued.

It should be noted that, in our junction scenario, it can happen that one quark has a low initial momentum in the junction rest frame, and therefore never strays very far away. The string between this quark and the junction need then not break, so that the quark ends up in the central baryon together with the junction, i.e. the quark and the junction effectively act as a unit. Seemingly this is akin to the scenario sketched above but, in the junction topology framework, it could only happen when the quark has low momentum in the junction rest frame, so again the key baryon would be low-momentum.

Other alternatives appear even more far-fetched. For instance, we see no possibility for a Δ-shaped topology, i.e. connecting each quark directly with the other two. Not only would it be even more energetically unfavourable relative to the junction topology, but it is also difficult to conceive of a colour assignment that would at all allow it. One would then need to introduce a novel kind of strings, that do not obey the normal QCD colour charge and flux quantization conditions.

4.3 Junction motion

In the rest frame of the junction the opening angle between any pair of quarks is 120°, i.e. we have a perfect Mercedes topology. This can be derived from the action of the classical string [27], but follows more directly from symmetry arguments. What is maybe not so obvious is that the 120° condition also is fulfilled if the quarks are massive. However, in the junction rest frame each string piece is pulled straight out from the origin, without any transverse motion, so the string pieces do not carry any momentum. Then overall momentum conservation gives that

$$\frac{\mathrm{d}\mathbf{p}_{\mathrm{tot}}}{\mathrm{d}t} = \sum_{\mathrm{q}} \frac{\mathrm{d}\mathbf{p}_{\mathrm{q}}}{\mathrm{d}t} = -\kappa \sum_{\mathrm{q}} \mathbf{e}_{\mathrm{q}} = \mathbf{0} \; . \tag{8}$$

Here we have used eq. (4) to give the momentum loss of quarks of arbitrary mass, where $\mathbf{e}_{\mathrm{q}}$ is a unit vector along the direction of motion of each of the three quarks.

The flow of energy and momentum is akin to that in the normal $\mathrm{q}\overline{\mathrm{q}}$ system, where the intermediate string absorbs and cancels the momentum of the receding q and $\overline{\mathrm{q}}$. With respect to the qqq case, it is implicit in eq. (8) that no net momentum is accumulated by the junction. Instead, it acts as a switchyard for the momentum flowing in the system, thereby cancelling the momentum given up by the three endpoint quarks. In this way, the junction itself remains with a vanishing four-momentum, which obviously holds in an arbitrary reference frame. In a general frame the string pieces would have a transverse motion as well, however, and thereby carry a nonvanishing momentum. Then eq. (8) would need to be generalized to include these additional terms and would become less transparent.

The rest frame of the junction can easily be found for the case of three massless quarks (and no further gluons), but the general massive case admits no analytical solution. A convenient numerical solution can be obtained as follows. Imagine three quarks with four-momenta p_1, p_2 and p_3. The four-products $a_{ij} = p_i p_j$ are Lorentz invariants, and thus the boosted momenta p'_i obey

$$a_{ij} = p'_i p'_j = E'_i E'_j - \mathbf{p}'_i \mathbf{p}'_j = E'_i E'_j - |\mathbf{p}'_i|\,|\mathbf{p}'_j| \cos\frac{2\pi}{3} = E'_i E'_j + \frac{1}{2}\,|\mathbf{p}'_i|\,|\mathbf{p}'_j| \tag{9}$$

in the junction rest frame. This leads us to introduce

$$f_{ij} \equiv f(|\mathbf{p}'_i|, |\mathbf{p}'_j|; m_i, m_j, a_{ij}) = \sqrt{|\mathbf{p}'_i|^2 + m_i^2}\sqrt{|\mathbf{p}'_j|^2 + m_j^2} + \frac{1}{2}|\mathbf{p}'_i|\,|\mathbf{p}'_j| - a_{ij} \ . \qquad (10)$$

Note that f_{ij} is a monotonically increasing function of each of its first two arguments. If we choose e.g. to let $|\mathbf{p}'_1|$ vary freely within the kinematically allowed region, the requirements $f_{12} = 0$ and $f_{13} = 0$ can then be uniquely solved to give the other two momenta,

$$|\mathbf{p}'_j| = \frac{2E'_1\sqrt{4a_{1j}^2 - m_j^2(4{E'_1}^2 - |\mathbf{p}'_1|^2)} - 2|\mathbf{p}'_1|\,a_{1j}}{4{E'_1}^2 - |\mathbf{p}'_1|^2} \ , \qquad (11)$$

which both decrease with increasing $|\mathbf{p}'_1|$. Therefore also f_{23} is monotonically decreasing if viewed as a function of $|\mathbf{p}'_1|$, $f_{23} = f(|\mathbf{p}'_2|(|\mathbf{p}'_1|), |\mathbf{p}'_3|(|\mathbf{p}'_1|))$ The final requirement $f_{23} = 0$ now gives a unique solution $|\mathbf{p}'_1|$. This solution can be obtained by an iterative interpolating procedure. In the massless case, the solution simplifies to $E'_i = |\mathbf{p}'_i| = \sqrt{2a_{ij}a_{ik}/3a_{jk}}$.

Once the energies in the junction rest frame are known, the construction of a boost is straightforward. A first boost with $\boldsymbol{\beta}^{\mathrm{CM}} = -\sum \mathbf{p}_i / \sum E_i$ brings the three quarks to their rest frame, with known momenta p_i^{CM}. A second boost $\boldsymbol{\beta}'$, that brings the system to the junction rest frame, now obeys the three equations $\gamma' E_i^{\mathrm{CM}} + \gamma'\boldsymbol{\beta}'\mathbf{p}_i^{\mathrm{CM}} = E'_i$. After division by E_i^{CM}, and subtraction of two of the equations from the third, one obtains e.g.

$$\gamma'\boldsymbol{\beta}' \left(\frac{\mathbf{p}_1^{\mathrm{CM}}}{E_1^{\mathrm{CM}}} - \frac{\mathbf{p}_j^{\mathrm{CM}}}{E_j^{\mathrm{CM}}} \right) = \frac{E'_1}{E_1^{\mathrm{CM}}} - \frac{E'_j}{E_j^{\mathrm{CM}}} \ . \qquad (12)$$

Since the three vectors $\mathbf{p}_i^{\mathrm{CM}}$ lie in a plane, the boost vector can be parameterized as a linear sum of the two difference vectors defined by the above equation for $j = 2$ and 3, which gives a simple linear equation system for $\gamma'\boldsymbol{\beta}'$. Finally, the overall boost is obtained by combining $\boldsymbol{\beta}^{\mathrm{CM}}$ with $\boldsymbol{\beta}'$.

In the general case, there does not have to exist a solution with perfect symmetry. Such troublesome events, characterized e.g. by $f_{23} < 0$ for all $|\mathbf{p}'_1|$, are very rare, however. We have only encountered them when a massive quark is almost at rest in the frame that comes closest to giving a symmetrical topology. We here accept an imperfect solution somewhere in the neighbourhood of this singular point. Since it is the size of the boost that will matter in the hadronization description, not the 120° opening angles *per se*, this should be acceptable.

So far we have assumed that the junction remains in uniform motion. When gluon emission is included, this need no longer be the case. Consider e.g. an event like the one in Fig. 5. Here the two $\mathrm{d}_{(j,k)}$ quarks each radiated a gluon, and so the strings from these quarks to the junction are drawn via the respective gluon, cf. Fig. 2. It is the direction of these gluons, together with the u quark, that determines the junction motion at early times, and the directions of the $\mathrm{d}_{(j,k)}$ quarks themselves are irrelevant. As a gluon moves out from the junction origin, it loses energy at a rate $\mathrm{d}E/\mathrm{d}t = -2\kappa$, where the 2 comes from it being attached to two string pieces. So after a time $E_{\mathrm{g}}(0)/2\kappa$ it has lost all its original energy, and after a further equal time this information has propagated back to the junction. From then on it would be the direction of the respective $\mathrm{d}_{(j,k)}$ quark, and not of the gluon, that defines the pull on the junction. In the example of Fig. 5, the junction would originally be at rest but later on start to move leftwards. In the generic configuration, each of the outgoing quarks could radiate several gluons, that would be colour-connected in a chain stretching from the endpoint quark inwards to the junction.

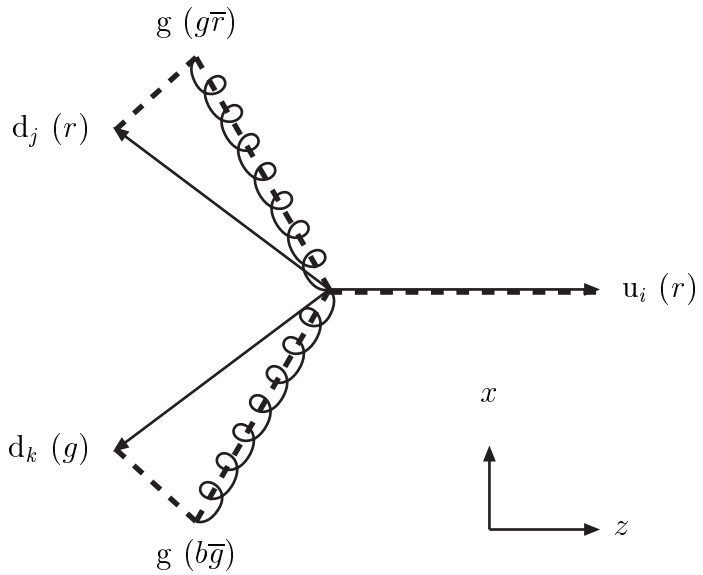

Figure 5: String topology of a $\tilde{\chi}_1^0 \to \mathrm{u}_i\mathrm{d}_j\mathrm{d}_k$ decay, where the two $\mathrm{d}_{(j,k)}$ quarks each has radiated a gluon. The event is drawn in the rest frame of the junction at early times, where the u and the two gluons are separated by 120°, and the string topology is shown by dashed lines. A possible colour assignment is indicated within brackets.

The innermost gluon on each of the three chains would together determine the original motion, with the next-innermost taking over after the innermost lost its energy, and so on, spreading outwards. As a consequence the junction would "jitter around".

Now, all of this is moot if the string starts to fragment before the innermost gluon lost its energy, because a string break will sever the inward flow of momentum. As we noted above, the typical scale for this to happen is of order $\langle\kappa\tau\rangle \approx 1.5$ GeV. Therefore an innermost gluon with energy much above this scale by itself defines the junction motion, whereas a gluon with energy much below would act on the junction too short a time to matter.

Rather than trying to trace the junction jitter in detail — which anyway will be at or below the limit of what it is quantum mechanically meaningful to speak about — we define an effective pull of each string on the junction as if from a single particle with a four-momentum

$$p_{\mathrm{pull}} = \sum_{i=1}^{n} p_i \, \exp\left(-\textstyle\sum_{j=1}^{i-1} E_j / E_{\mathrm{norm}}\right) \quad . \tag{13}$$

Here $i = 1$ is the innermost gluon, $i = 2$ is the next-innermost one, and so on till the endpoint quark $i = n$. The energy sum in the exponent runs over all gluons inside the one considered (meaning it vanishes for $i = 1$), and is normalized to a free parameter E_{norm}, which by default we associate with the $\langle\kappa\tau\rangle$ above. Note that the energies E_j depend on the choice of frame. A priori, it is the energies in the rest frame of the junction which should be used in this sum, yet since these are not known to begin with, we use an iterative procedure, starting with the (known) energies in the CM of the string system, calculating the corresponding pull vectors in this frame and from them the candidate junction rest frame, calculating the pull vectors in this new frame and so forth until the Lorentz factor of the last boost is $\gamma_{\mathrm{last}} < 1.01\gamma_{\mathrm{tot}}$.

4.4 Junction hadronization

As we have noted above, hadronization begins in the middle of an event and spreads outwards. In the junction rest frame the junction baryon would thus be the one to form first, on the average, and have a rather small momentum. Thereafter, each of the three strings would fragment pretty much as ordinary strings, e.g. as in a back-to-back $q\overline{q}$ pair of jets. Also extensions to systems with multiple gluon emissions should closely follow the corresponding pattern for normal events. With or without gluon emission, we shall speak of three strings connected at the junction, where a string may consist of several string pieces between adjacent (i.e. colour-connected) partons.

In particular, if we consider events where each of the three outgoing quark jets have large energies in the junction rest frame, the production of high-momentum particles inside a jet should agree with the one of a corresponding jet in an ordinary two-jet event. This can be ensured by performing the fragmentation from the outer end of the strings inwards, just like for the $q\overline{q}$ string. Thus an iterative procedure can be used, whereby the leading q is combined with a newly produced $\overline{q}_1$, to form a meson and leave behind a remainder-jet q_1, which is fragmented in its turn. Flavour rules, fragmentation functions and handling of gluon-emission-induced kinks on the string are identical with the ones of the ordinary string.

While these hadronization principles as such are clear, and give the bulk of the physics, unfortunately there is a catch: if all three strings are fragmented until only little energy and momentum remain in each, and then these remainders are combined to a central baryon, what guarantees that this baryon obtains the correct invariant mass it should have?

The same problem exists in simple $q\overline{q}$ events, that also there energy and momentum is not guaranteed to come out right, if the event is fragmented independently from the two ends and then joined by a single hadron in the middle. In this case, the overall energy–momentum conservation is obtained by the "area law" [21], which couples the production of *all* the hadrons in the event. It is therefore difficult to simulate exactly, but for large remaining invariant masses it simplifies to the iterative framework already introduced. For small masses a pragmatic approximation is used. Firstly, not one but two hadrons are used to join the jets. A two-hadron system has a continuous mass spectrum, so one may construct consistent kinematics if the normal fragmentation is stopped when the remaining invariant mass has dropped below some value. Since the final two hadron masses are not known beforehand, sometimes the remaining mass drops below the two-body threshold, in which case the fragmentation is re-started from the beginning. Secondly, by a random choice of producing the next hadron either off the q end or off the $\overline{q}$ one, the final joining does not always occur exactly in the middle of events, thereby smearing remaining imperfections of the joining procedure proper.

For the fragmentation of a junction topology, we attempt to retain as much as possible the known good features of the existing approach to $q\overline{q}$ events, although this involves conflicting interests, as follows. In order to describe the production of high-momentum particles, fragmentation should be allowed to proceed from all three string ends inward. But, in order not to bias the junction baryon overly, the joining for energy-momentum conservation should not always have to influence this hadron. Briefly put, the solution is to fragment two of the three strings inwards, thereafter combine their leftovers to an effective diquark, and finally fragment the string between this diquark and the third end in much the same spirit as described for $q\overline{q}$ events above, i.e. by fragmentation at random off both ends of the system. Put in the context of Fig. 4, imagine first tracing the chains

$\mathrm{d}_j - \mathrm{q}_5 - \mathrm{q}_6 - \mathrm{q}_7$ and $\mathrm{d}_k - \mathrm{q}_8 - \mathrm{q}_9$, then forming a diquark $\mathrm{q}_7\mathrm{q}_9$, and thereafter fragmenting the string between this diquark and u from both ends.

There are a number of technical details, as follows. The hadronization process itself is normally carried out in the rest frame of the colour singlet system under consideration, but is Lorentz covariant, so another choice would be no problem. Information on the junction motion is encoded in its velocity four-vector $v_{\mathrm{jun}} = (\gamma', -\gamma'\boldsymbol{\beta}')$, with the $\boldsymbol{\beta}'$ defined in subsection 4.3.

For normal string pieces, spanned between two partons, the invariant mass of the piece is defined by the four-momenta of the two endpoint partons. Since the junction does not carry a momentum, there is no corresponding definition for the string pieces spanned between the junction and each of its three nearest colour-connected partons. Instead the junction end is here represented by a fictitious parton, specific to each string, opposite to the p_{pull} vector of eq. (13), as viewed in the junction rest frame, which gives $p_{\mathrm{opp}} = -p_{\mathrm{pull}} + 2(v_{\mathrm{jun}}p_{\mathrm{pull}})v_{\mathrm{jun}}$.

Two of the three strings are fragmented from the respective end inwards, towards a fictitious other end as defined above. In order to have a large-mass system left for the system in which the joining occurs, we prefer to pick these two to be the ones with lowest energy, as defined in the junction rest frame, i.e. with lowest $E'_{\mathrm{str}} = v_{\mathrm{jun}} \sum_i p_i^{\mathrm{CM}}$. Here p_i are the four-momenta of the partons belonging to the given string, excluding the fictitious junction one. As the hadrons are successively produced, their summed energy E'_{had} (in the same frame) is also updated. Once the hadronic energy exceeds the string one, $E'_{\mathrm{had}} > E'_{\mathrm{str}}$, the process has gone too far, i.e. passed the junction point of the string system, so it is stopped and the latest hadron is rejected.

The random choices made in the fragmentation function allows the energy in this latest hadron to fluctuate significantly. It can therefore be that, after its removal, the energy $\delta E' = E'_{\mathrm{str}} - E'_{\mathrm{had}}$ remaining of a string can be quite significant. This is particularly dangerous if it happens in both of the strings considered, since then the leftovers would be combined to give a momentum intermediate in direction to the two strings, and thereby maybe give a jet where none originally existed. Therefore the two hadronic chains are rejected and new ones are generated in their place if both $\delta E'$ are larger than a parameter $\delta E'_{\mathrm{min}}$, by default 1 GeV. One of the two can have a larger energy than this, since then the combined leftovers would still essentially agree with the direction of this original string, but the chains are also rejected if this one has an energy above $\delta E'_{\mathrm{min}} + R\,\delta E'_{\mathrm{max}}$, where $\delta E'_{\mathrm{max}}$ by default is 10 GeV and R is a random number uniformly selected between 0 and 1. The two parameters $\delta E'_{\mathrm{min}}$ and $\delta E'_{\mathrm{max}}$ are "tuned" by the requirements of a consistent description, see below. In order to avoid infinite loops, at most 10 attempts of the above kind are rejected.

When two acceptable hadronic chains have been found, the remaining four-momenta from the respective two strings are combined into a single parton, which then replaces the junction as endpoint for the third string. (Actually, technically, the whole of the two string four-momenta is assigned to a parton, but then the fragmentation process is assumed already to have produced the given set of hadrons. This is almost equivalent, apart from some minor details of transverse momentum handling.) The new effective parton may have a larger momentum than energy, and thereby nominally be spacelike. If only by a little, it normally would not matter, but in extreme cases the whole final string may even come to have a negative squared mass. Therefore additional checks are made to ensure that the final string mass is above the threshold for string fragmentation. If so, the fragmentation procedure is identical with that of an ordinary string from here on, else repeated attempts are made, starting over with the first two strings.

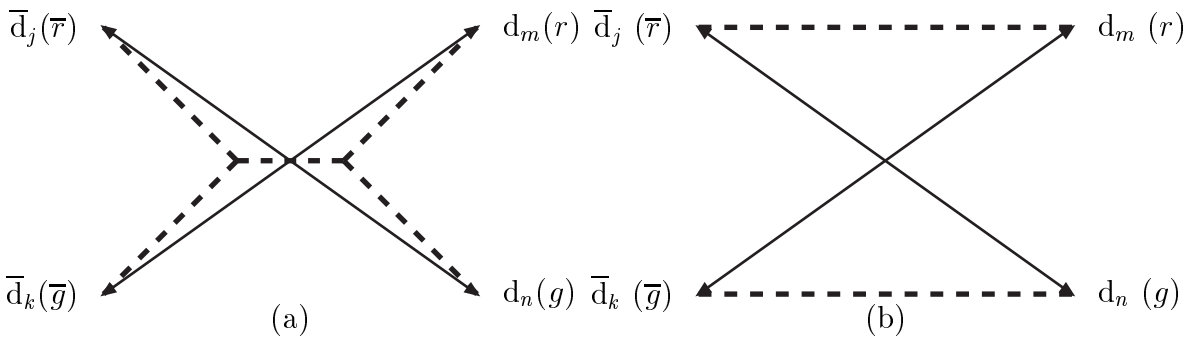

Figure 6: (a) Schematic string topology of a $\mathrm{e^+e^-} \to \tilde{\mathrm{t}}\tilde{\mathrm{t}}^* \to \overline{\mathrm{d}}_j\overline{\mathrm{d}}_k\mathrm{d}_m\mathrm{d}_n$ decay. The strings are shown as dashed lines. A possible colour assignment is indicated within brackets. The string between the two junctions would then be blue–antiblue. (b) Alternative string drawing for the same process, without any junctions.

A further aspect is the flavour properties. Except at the junction, the normal rules of string fragmentation are used. At the junction, the two strings fragmented first each define a leftover quark, which are combined into a diquark. This diquark is assigned a spin 0 or 1 according to the same relative probabilities as normally. Since also ordinary fragmentation can produce diquark–antidiquark pairs, it could be that either string ends with a leftover antidiquark rather than quark. Such configurations are not acceptable, and have to be rejected in favour of new tries. Once a diquark is defined, this can fragment further as usual. In the simplest scenario, it will next fragment to produce a baryon and a leftover antiquark. If popcorn baryon production is allowed, however, a meson may alternatively be split off to produce a new diquark. That is, the baryon number may then migrate to higher energies than otherwise, but will still be rather centrally produced.

4.5 Other string topologies

So far we have considered the production of string systems containing a single junction, well illustrated by the case of neutralino decays, but also possible in other processes. There is a second possibility, however, namely that of a system consisting of two junctions, or, more precisely, of a junction and an antijunction, where the former is associated with a baryon number $+1$ and the latter -1. An example would be $\mathrm{e^+e^-} \to \tilde{\mathrm{t}}\tilde{\mathrm{t}}^* \to \overline{\mathrm{d}}_j\overline{\mathrm{d}}_k\mathrm{d}_m\mathrm{d}_n$, containing two BNV decays, $\tilde{\mathrm{t}} \to \overline{\mathrm{d}}_j\overline{\mathrm{d}}_k$ and $\tilde{\mathrm{t}}^* \to \mathrm{d}_m\mathrm{d}_n$. This kind of topology is illustrated in Fig. 6a. There are now two quark ends, two antiquark ones, and five strings, including the one between the two junctions. Each of these strings could contain an arbitrary number of intermediate gluons, where gluons in between the two junctions are related to emission in the production process $\mathrm{e^+e^-} \to \tilde{\mathrm{t}}\tilde{\mathrm{t}}^*$ and the others to the decay processes (with the standard ambiguities, especially relevant for the soft gluons).

The junction motion and string fragmentation follows by simple generalization of what has already been discussed for configurations with a single junction. Like before, two of the three strings from a junction — the two not connected to the other junction — are first fragmented, and the leftovers combined to an effective (anti)diquark. When this has been performed for both junctions, what remains is a diquark–antidiquark string spanned between the two junctions, which then is fragmented. Thus the hadronization will produce one baryon and one antibaryon, associated with the junctions, plus potentially additional

baryon–antibaryon pairs as usual.

The same checks as above have to be applied at various stages, but no new ones. The one ambiguity is how to calculate the $p_{\rm pull}$ of eq. (13) for the third string of a junction, hooking up to the other junction. Here gluons on the string between the two junctions are considered as normally, while partons on the far side of the other junction are tracked down each of the two strings without including any exponential suppression from energies in the other of the strings.

Since the net baryon number vanishes in the above topology, an alternative string scenario is illustrated by Fig. 6b. Here two strings are pulled directly between a $\mathrm{d}_{(m,n)}$ and a $\overline{\mathrm{d}}_{(j,k)}$ quark. The junctions are gone, and so such an event would not have to contain any baryons or antibaryons at all, and definitely not any associable with the BNV processes as such. This is the approach adopted in HERWIG.

A priori, one does not know which of the two above scenarios would be the correct one. It would not even have to be a unique answer, valid for all events. A possibility would be that the topology with minimal string length is selected dynamically. Then events of the general kind shown in Fig. 6 would obtain the 2-junction topology of Fig. 6a when the $\mathrm{d}_m\mathrm{d}_n$ and $\overline{\mathrm{d}}_j\overline{\mathrm{d}}_k$ opening angles are small, while the 0-junction one of Fig. 6b would result if instead the $\mathrm{d}_m\overline{\mathrm{d}}_j$ and $\mathrm{d}_n\overline{\mathrm{d}}_k$ opening angles were the small ones.

Such a simple picture would become more complicated by the addition of gluons in the production process, i.e. the ones we above put on the string between the two junctions. It now becomes necessary to subdivide such gluons into two separate colour lines, one between each of the outgoing $\mathrm{d}_{(m,n)}\overline{\mathrm{d}}_{(j,k)}$ pairs. In general, we would expect the 0-junction topology to become more disfavoured when there are several gluons being emitted.

Furthermore, in the limit of large $\tilde{\mathrm{t}}$ lifetime, the string between the $\tilde{\mathrm{t}}$ and $\tilde{\mathrm{t}}^*$ would have time to start to fragment before the $\tilde{\mathrm{t}}$ or $\tilde{\mathrm{t}}^*$ has decayed. In such a case, the event would consist of two separate colour singlets, that fragment independently of each other. This does not have to mean timescales long enough to have multiple string breaks and the formation of stop-hadrons: one single string break is enough to make the production of a baryon and an antibaryon unavoidable. At first glance a sufficiently large lifetime for this to happen, $c\tau \gtrsim 1$ fm, would seem unlikely. However, when only BNV decay channels are kinematically allowed, the $\tilde{\mathrm{t}}$ lifetime is almost always non-negligible, since, for massless d, s, and b quarks the decay length is roughly:

$$c\tau_{\tilde{\mathrm{t}}}^{\mathrm{BNV}} \approx (100\ \mathrm{fm}) \times \left(\frac{0.01}{|\lambda''_3|}\right)^2 \times \frac{100\ \mathrm{GeV}}{m_{\tilde{\mathrm{t}}}} \tag{14}$$

where $|\lambda''_3|$ represents the average of the $|\lambda''_{3jk}|$ couplings. Strictly speaking, the above formula is valid for $\tilde{\mathrm{t}}_R$. For $\tilde{\mathrm{t}}_1$ ($\tilde{\mathrm{t}}_2$), it is increased by $1/|\sin\theta_{\tilde{\mathrm{t}}}|^2$ ($1/|\cos\theta_{\tilde{\mathrm{t}}}|^2$). In passing, we note that event properties are likely to be similar whether stop-hadrons have time to be produced or not: corresponding studies for ordinary top quarks have shown that differences are restricted to the region of low-momentum particles, and there mainly show up in angular distributions, not averaged event properties [34].

If gauge-interaction decay channels such as $\tilde{\mathrm{t}} \to \mathrm{b}\tilde{\chi}_1^+$ are open, these will almost always dominate. Then, ignoring what happens to the colour disconnected $\tilde{\chi}_1^+$, it would be doubly rare to have both $\tilde{\mathrm{t}}$ and $\tilde{\mathrm{t}}^*$ decay with BNV. Experimental studies would presumably have to concentrate on finding events where one decay is BNV and the other not, and so we are back with a 1-junction topology.

Finally, we note that $\tilde{\mathrm{t}}\tilde{\mathrm{t}}^*$ production in hadron colliders would predominantly come from $\mathrm{gg} \to \tilde{\mathrm{t}}\tilde{\mathrm{t}}^*$ in the colour octet channel, where thereby the $\tilde{\mathrm{t}}$ and $\tilde{\mathrm{t}}^*$ would belong to

separate colour singlet subsystems. Again the production of a baryon and an antibaryon would then be inevitable.

Nevertheless, in order to test the consequences, we have developed an alternative model. For a given event with two colour-connected BNV decays, the total string length is evaluated under the assumption that the event either is arranged in a 2-junction or in a 0-junction topology, and the topology is chosen that corresponds to the smallest length. Given this choice the subsequent hadronization is well-defined.

In more detail, the string length is defined by the so-called λ measure [35]. For a simple two-parton system

$$\lambda = \ln\left(\frac{s}{m_0^2}\right) \quad . \tag{15}$$

Here s is the squared invariant mass of the system and m_0 is some hadronization reference scale of order $\langle\kappa\tau\rangle$, just like the $E_{\rm norm}$ defined in section 4.3. Particles are produced with a flat rapidity distribution in the central regions of the string, while the distribution falls off near the ends. Then $y_{\rm max} \simeq \ln(\sqrt{s}/m_0)$ defines the effective rapidity range, in the middle of the fall-off, such that the total multiplicity on the average is proportional to $y_{\rm max}$. For a generic string configuration, with many gluons between the quark and antiquark, the complete λ expression is rather messy, but approximately it can be represented by the linear sum of the λ measure for each string piece,

$$\lambda = \sum_{i=1}^{n-1} \lambda_{i,i+1} = \sum_{i=1}^{n-1} \ln\left(\frac{s_{i,i+1}}{m_0^2}\right) \quad . \tag{16}$$

Here the squared invariant mass $s_{i,i+1}$ is calculated with the full momentum for the end-point quarks but only half for the intermediate gluons, which are shared between two adjacent string pieces.

We now need to generalize the λ measure to the case with junctions, which has not been considered in the literature so far. To begin, revert to a simple back-to-back $\mathrm{q\overline{q}}$ system, with quark masses negligible. Then

$$\lambda = \ln\left(\frac{s}{m_0^2}\right) = \ln\left(\frac{4E_{\rm q}E_{\overline{\rm q}}}{m_0^2}\right) = \ln\left(\frac{2E_{\rm q}}{m_0}\right) + \ln\left(\frac{2E_{\overline{\rm q}}}{m_0}\right) = \ln\left(\frac{2vp_{\rm q}}{m_0}\right) + \ln\left(\frac{2vp_{\overline{\rm q}}}{m_0}\right) \quad . \tag{17}$$

The splitting into two terms can be seen as a separation of the full rapidity range into one on the quark side of the event and another on the antiquark one, smoothly matching at the origin. At this stage the origin is arbitrary, i.e. $E_{\rm q} \neq E_{\overline{\rm q}}$ represents an event boosted along the event axis; the individual terms may thus be changed but the sum remains invariant. In the final step the origin is represented by the four-vector $v = (1; 0, 0, 0)$, to allow a Lorentz invariant form also for the split expression. Alternatively to considering $E_{\rm q} \neq E_{\overline{\rm q}}$ one may then use a v boosted along the event axis.

In a $\mathrm{q_1q_2q_3}$ event, if viewed in the rest frame of the junction, there will be three rapidity plateaus extending from the origin, so one can calculate a total rapidity range

$$\lambda = \ln\left(\frac{2vp_1}{m_0}\right) + \ln\left(\frac{2vp_2}{m_0}\right) + \ln\left(\frac{2vp_3}{m_0}\right) \quad . \tag{18}$$

The v four-vector now is easily identified with the motion of the junction.

We also need to consider the rapidity length of the string between two junctions. Since the rapidity plateau extends all the way to the junction, this is actually given by

the rapidity difference between the junctions themselves. Evaluating this in a frame where the junctions are back-to-back, $v_{1,2} = (\gamma; 0, 0, \pm\gamma\beta)$, one obtains

$$\lambda = 2y_{\max} = 2\frac{1}{2}\ln\left(\frac{\gamma+\gamma\beta}{\gamma-\gamma\beta}\right) = \ln\left(\frac{1+\beta}{1-\beta}\right) = \ln\left(\frac{1+\beta^2+2\beta}{1-\beta^2}\right) \ , \tag{19}$$

with $v_1 v_2 = \gamma^2(1+\beta^2) = (1+\beta^2)/(1-\beta^2)$ or $\beta^2 = (v_1 v_2 - 1)/(v_1 v_2 + 1)$.

We can now give the λ of the two configurations in Fig. 6a and 6b. Since the number of m_0 factors agrees between the two, it is more convenient to introduce $\Lambda = m_0^4 \exp(\lambda)$, with expressions

$$\Lambda_{2-\text{junction}} = (2v_1p_m)(2v_1p_n)(2v_2p_j)(2v_2p_k)\left(v_1v_2 + \sqrt{(v_1v_2)^2-1}\right) \ , \tag{20}$$

$$\Lambda_{0-\text{junction}} = (2p_mp_j)(2p_np_k) \ , \tag{21}$$

where we have reused the generation indices of the quarks to distinguish them, and v_1 (v_2) corresponds to the right (left) vertex. The smaller of the two Λ values now determines which configuration would be the preferred one. Note that both expressions are linear in each of the p_i, so the choice only depends on the directions of motion of the outgoing quarks.

Now consider the complications caused by showering. Radiation after the BNV decays is no problem: one only needs consider the connection out to the colour produced in the BNV decays, i.e. to the gluon nearest to the junction, since the subsequent colour chain out to the endpoint quark would be unaffected by the colour arrangement between the two BNV vertices. The $p_{j,k,m,n}$ in eqs. (20)–(21) should be redefined accordingly. Radiation patterns before the BNV decays can be divided into two classes.

(i) If the shower contains a $\mathrm{g} \to \mathrm{q\overline{q}}$ branching, the colour flow in the system is automatically broken, and then the production of a baryon–antibaryon pair is unavoidable. This is the perturbative equivalent of the string between $\tilde{\mathrm{t}}$ and $\tilde{\mathrm{t}}^*$ starting to fragment before the $\tilde{\mathrm{t}}$ or $\tilde{\mathrm{t}}^*$ has decayed. As one moves up from the kinematical threshold this probability increases. Since the collinear and soft gluon singularities are tamed by the large $\tilde{\mathrm{t}}$ mass and width, the total $\mathrm{g} \to \mathrm{q\overline{q}}$ probability is reasonably reliably predictable, although a cut-off dependence e.g. from the assumed effective quark masses remains.

(ii) If there are no $\mathrm{g} \to \mathrm{q\overline{q}}$ branchings, all the gluons in the shower can be arranged in a single colour chain between the $\tilde{\mathrm{t}}$ and $\tilde{\mathrm{t}}^*$. When the BNV decays occur, the anticolour of the gluon that matches the colour of the $\tilde{\mathrm{t}}$ could no longer match the anticolour of either $\tilde{\mathrm{t}}$ decay product in a junction-free topology, but would rather have to be matched to the colour of either $\tilde{\mathrm{t}}^*$ decay product. Thus the 0-junction configuration would be with two strings, one between one of the $\tilde{\mathrm{t}}^*$ decay product traversing all the gluons from the original $\tilde{\mathrm{t}}$ edge to the $\tilde{\mathrm{t}}^*$ one and then zig-zagging back to one of the $\tilde{\mathrm{t}}$ decay products, while the other string would be between the two remaining decay products. See Fig. 7 for an illustration of (a) the 2-junction configuration and (b) the 0-junction one just discussed. (Actually, since the stop mass reduces collinear emission, and since the stop decay products are widely scattered, the zig-zag pattern need not be as extreme as one might guess at first glance.) Colour-suppressed topologies are neglected, such as where the gluons split off into a closed loop and then two strings are stretched directly between the $\tilde{\mathrm{t}}$ and $\tilde{\mathrm{t}}^*$ decay products. When comparing string length with and without junctions, the string internally between the intermediate gluons is common and can be neglected. Labelling by p_i the gluon closest to the v_i vertex in colour space, in the chain between

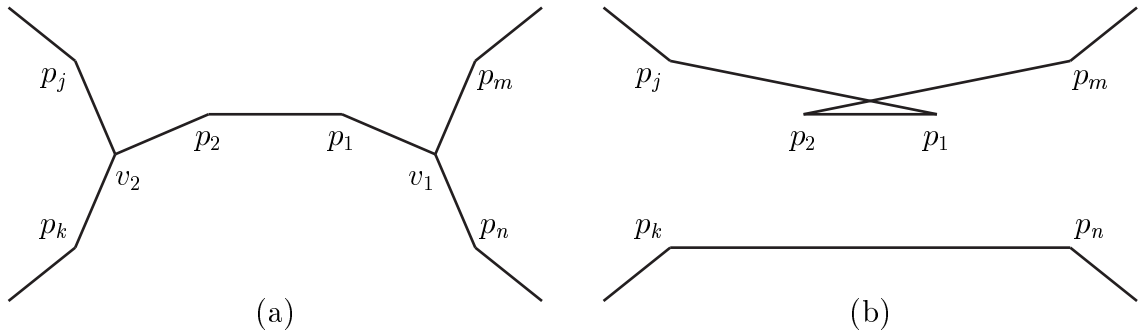

Figure 7: Illustration of (a) the 2-junction topology and (b) a 0-junction topology, for identical parton configurations. Indices have been chosen so as to correspond directly to the expressions in eqs. (22) and (23). Naturally, the topology in (b) only corresponds to one possible choice of which is which of (m,n) and (j,k).

the two junctions, and now putting $\Lambda = m_0^6 \exp(\lambda)$, one obtains

$$\Lambda_{2-\mathrm{junction}} = (2v_1p_m)(2v_1p_n)(2v_1p_1)(2v_2p_j)(2v_2p_k)(2v_2p_2) \; , \tag{22}$$

$$\Lambda_{0-\mathrm{junction}} = (2p_mp_2)(2p_jp_1)(2p_np_k) \; , \tag{23}$$

where which is which of m and n (and of j and k) is chosen at random.

If anything, the approach above could overestimate the probability of no baryon–antibaryon production, since it only considers the gain in string length once one has arrived at a new colour arrangement, whereas there could be additional dynamic suppressions on the way between the 'original' 2-junction topology and the 'final' 0-junction one. Nevertheless, it should offer some realistic estimates how big a loss of baryon signal could at worst be. To quantify this to some extent, we have taken a closer look at isolated decays of $\tilde{\mathrm{t}}\tilde{\mathrm{t}}^*$ pairs (colour connected to each other to form an overall colour singlet) in the CM of the pair.

For high-momentum stops, $\gamma_{\tilde{\mathrm{t}}} \equiv E_{\mathrm{CM}}/2m_{\tilde{\mathrm{t}}} \gg 1$, the $\mathrm{d}_m\mathrm{d}_n$ pair lies at a large rapidity separation from the $\overline{\mathrm{d}}_j\overline{\mathrm{d}}_k$ pair. In the 2-junction topology, this rapidity range is spanned by *one* string piece, the junction–junction one, whereas, in the 0-junction topology, *each* of the $\mathrm{d}\overline{\mathrm{d}}$ string pieces must cross it. In fact, due to the see-saw nature of the 0-junction topology in the presence of gluon radiation from the stops, the central rapidity range will be crossed more than twice if the stops radiate. Thus, we expect the 2-junction topology to dominate for cases $\gamma_{\tilde{\mathrm{t}}} \gg 1$.

On the other hand, when the stops are slow, $\gamma_{\tilde{\mathrm{t}}} \sim 1$, the $\tilde{\mathrm{t}}$ and $\tilde{\mathrm{t}}^*$ decay products are widely spread by the decay kinematics. Typically the invariant mass between a $\tilde{\mathrm{t}}$ decay product and a $\tilde{\mathrm{t}}^*$ one will be smaller than that between the two products of the same $\tilde{\mathrm{t}}$ or $\tilde{\mathrm{t}}^*$, such that the 0-junction topology is guaranteed to give a smaller string length. Also for somewhat larger $\gamma_{\tilde{\mathrm{t}}}$, where one can start to speak of an event axis, decay products are often thrown into the opposite hemisphere, such that the central rapidity region need not be crossed at all in the 0-junction alternative. Thus, we expect the 0-junction topology to dominate for reasonably low $\gamma_{\tilde{\mathrm{t}}}$.

The rapidity arguments presented in the above two paragraphs closely follow the here defined string length measures, eqs. (20)–(23). However, we may alternatively use an argument based on the string motion itself. Recall that a junction is at rest when the opening angles between its three attached strings is 120°. Thus, if the opening angles between the motion of the $\tilde{\mathrm{t}}$ and its two decay products is 60° each, and correspondingly

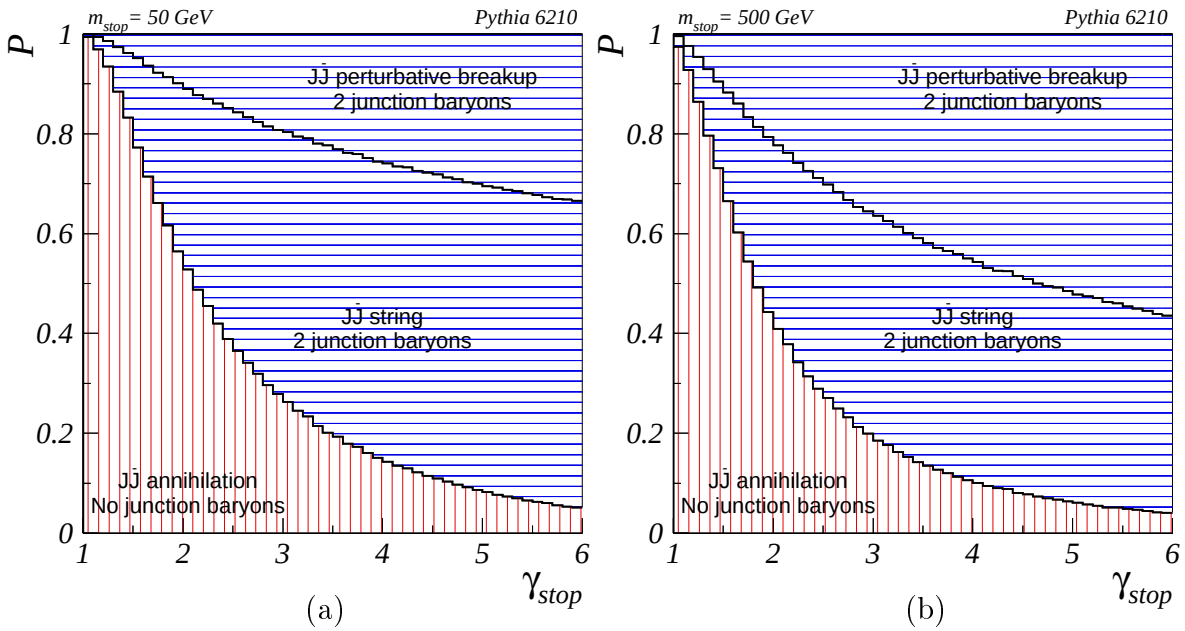

Figure 8: Probabilities for 2-junction and 0-junction configurations as functions of $\gamma_{\tilde{t}} = \frac{E_{\mathrm{CM}}}{2m_{\tilde{t}}}$ for (a) $m_{\tilde{t}} = 50$ GeV and (b) $m_{\tilde{t}} = 500$ GeV.

for the $\tilde{t}^*$, we are exactly at a balancing point. For stops faster than this, the smaller decay angles will force the two junctions to move away from each other, and so it should be less likely for them to meet and annihilate. For slower stops, the junctions actually move *towards* each other (if assumed produced at a distance apart), making it more believable that they can annihilate. Although these deliberations are separate from the string length minimization procedure described above, and do not give the same answer event by event, they do corroborate it by leading to the same expected dominant topologies as $\gamma_{\tilde{t}}$ is varied. The two approaches are about equally credible, but the string length argument has the advantage of leading to tractable answers also for quite complicated topologies.

Using now eqs. (20)–(23) to calculate total string lengths for two different stop masses, and a range of stop boosts $1 \leq \gamma_{\tilde{t}} \leq 6$, gives the plots shown in Fig. 8. As is apparent from the discussion above, we expect the ratio of 2-junction to 0-junction string topologies to depend mainly on $\gamma_{\tilde{t}}$ and only weakly on the stop mass as such, and this agrees with what is shown in the relation between the lower two regions of the plots. The feature which *does* change significantly is the rate of perturbative breakups of the 2-junction systems, i.e. $g \to q\overline{q}$ splittings in the parton shower initiated before the BNV decays, point *(i)* above. The $g \to q\overline{q}$ rate increases with larger total energy, also for fixed $\gamma_{\tilde{t}}$: while the primary emission rate of gluons off the $\tilde{t}\tilde{t}^*$ system is rather constant, the phase space for further cascading of these gluons is increased with energy.

5 Model tests

In this section we will present some distributions that illustrate the basic properties of our model, and show that it works as expected. In several cases we will compare with results obtained with Herwig, the other main complete implementation of BNV phenomenology. The distributions in this section are not necessarily directly observable; we will return to

experimental tests in the following section.

For calculating the sparticle mass and coupling spectrum, we use the mSUGRA parameters of Snowmass points 1a and 1b [36] input to ISASUSY [2] for RGE evolution. This is done for both HERWIG and PYTHIA, and so there can be no artifacts created by non-identical EW scale superspectra when comparing the output of the two programs. Apart from this aspect, most of the topics we study here are not sensitive to the details of the SUSY parameter set used.

For all studies, we use the "factory presets" for both PYTHIA and HERWIG. No tuning has been performed, and no demands e.g. of identical shower cut-offs or fragmentation functions have been made. This does mean that one must exercise a slight caution before drawing too strong conclusions from the comparisons, since default PYTHIA is not always directly comparable to default HERWIG. In the following, we will comment on these aspects when necessary.

5.1 Consistency checks

The main technical simplification of the junction string fragmentation scheme is the asymmetric fashion in which two of the three strings are first fragmented inwards, with the remnants joined to an effective diquark jet that is fragmented together with the third string. In particular, the fear might be that the joined diquark could produce a spurious new jet intermediate to the directions of the two strings from which it inherits the left-over momenta. Therefore the fragmentation of a symmetric three-parton configuration is studied in Fig. 9. For the production of hadrons other than the junction baryon, an essentially perfect symmetry between the three jets is obtained, both in angular and in momentum variables. As could be expected, the situation is less perfect for the junction baryon itself. Indeed, it has a tendency to be produced in a direction intermediate to the first two jets considered, rather than along either of these two separate directions, while baryons in the third jet line up the way one would like. It should be noted that most of this effect occurs for baryons of intermediate momenta $|\mathbf{p}| \simeq 1$ GeV; at lower momenta everything is and should be close to isotropic, while those few baryons that have large momenta tend to be better aligned with the jet directions. The overall balance between the jets is good, with 32% of the junction baryons found in the angular range around the third jet, relative to 34% in each of the other two. The momentum spectra in the three jets also show reasonable agreement: although the third tends to produce somewhat harder junction baryons than the first two, the difference only corresponds to a mean momentum of 0.97 GeV rather than of 0.87 GeV.

We may therefore conclude that the asymmetric algorithm does not seem to induce any imperfections in the bulk of the hadron production, and only rather modest ones for the junction baryon itself. These latter imperfections should also largely average out in realistic simulations, when the order in which jets have been hadronized is not known. Specifically, it appears to be a stable and reliable prediction of the model that the junction baryon should be found at low momentum, $|\mathbf{p}| \lesssim 2$ GeV, in the junction rest frame.

Further technical details, concerning the junction motion (subsection 4.3) and hadronization (subsection 4.4), could have been addressed in different approximations. Specifically, we have investigated how the fragmentation spectra would be affected if we made the following changes to our model:

1. Switched the order of fragmentation of the three string pieces, so that the *last* string to be fragmented would be the one containing *least* energy, the reverse of the default behaviour.

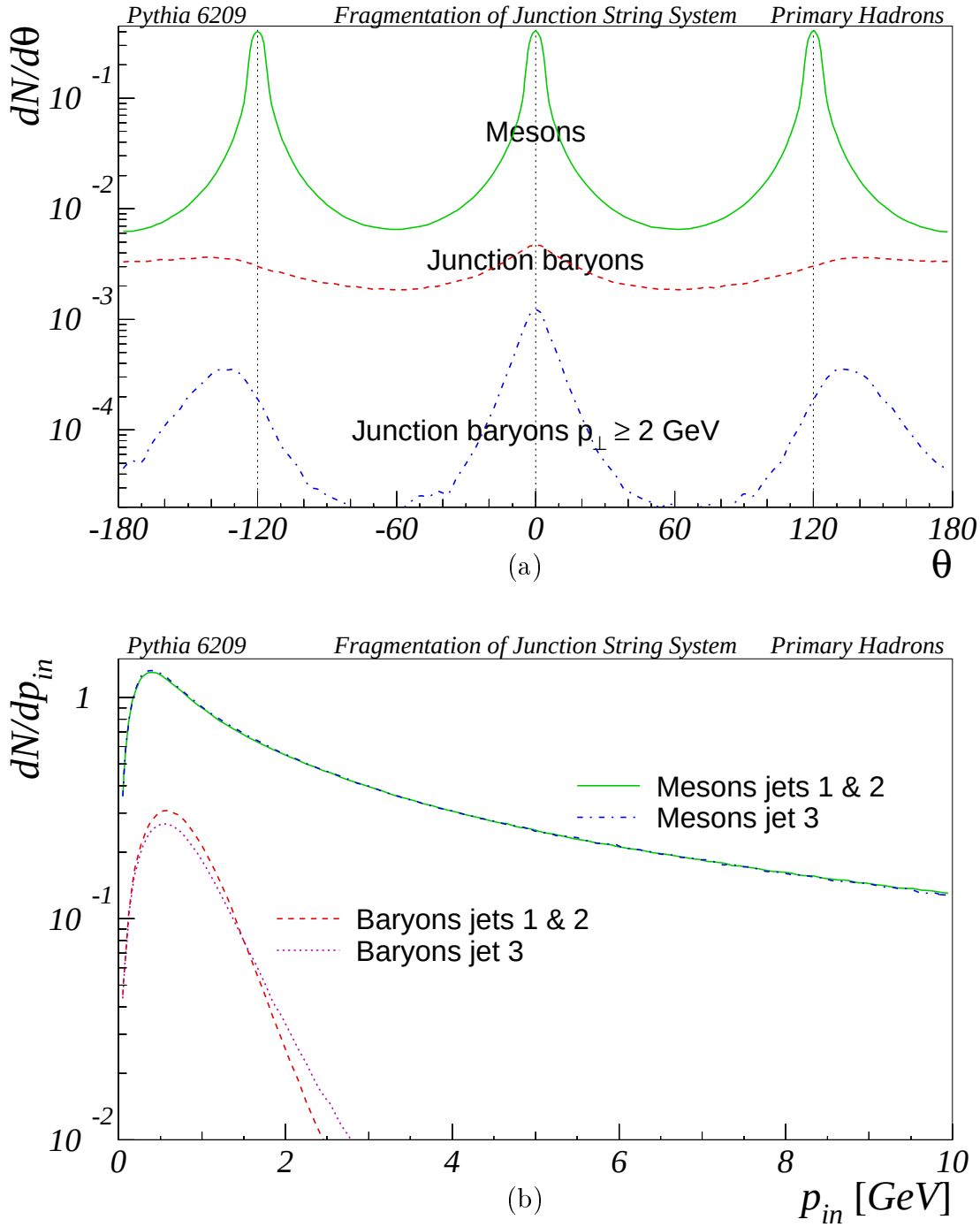

Figure 9: Fragmentation of a uuu parton configuration with 40 GeV in each jet and opening angles 120° between partons. Only the primary hadrons are shown, i.e. subsequent decays are disregarded. For simplicity all normal baryon–antibaryon production is switched off, as is the popcorn baryon possibility. (a) The particle flow $\mathrm{d}N/\mathrm{d}\theta$ in the event plane, for mesons, for the junction baryons and for the fraction of junction baryons with momentum in the event plane above 2 GeV. The jet at around 0° is the last one to be considered in the hadronization process. (b) The meson and junction baryon momentum spectra per jet, shown separately for the first two jets considered and for the last one. Hadron assignment to jets is based on a simple division of the plane into three equal 120° sectors.

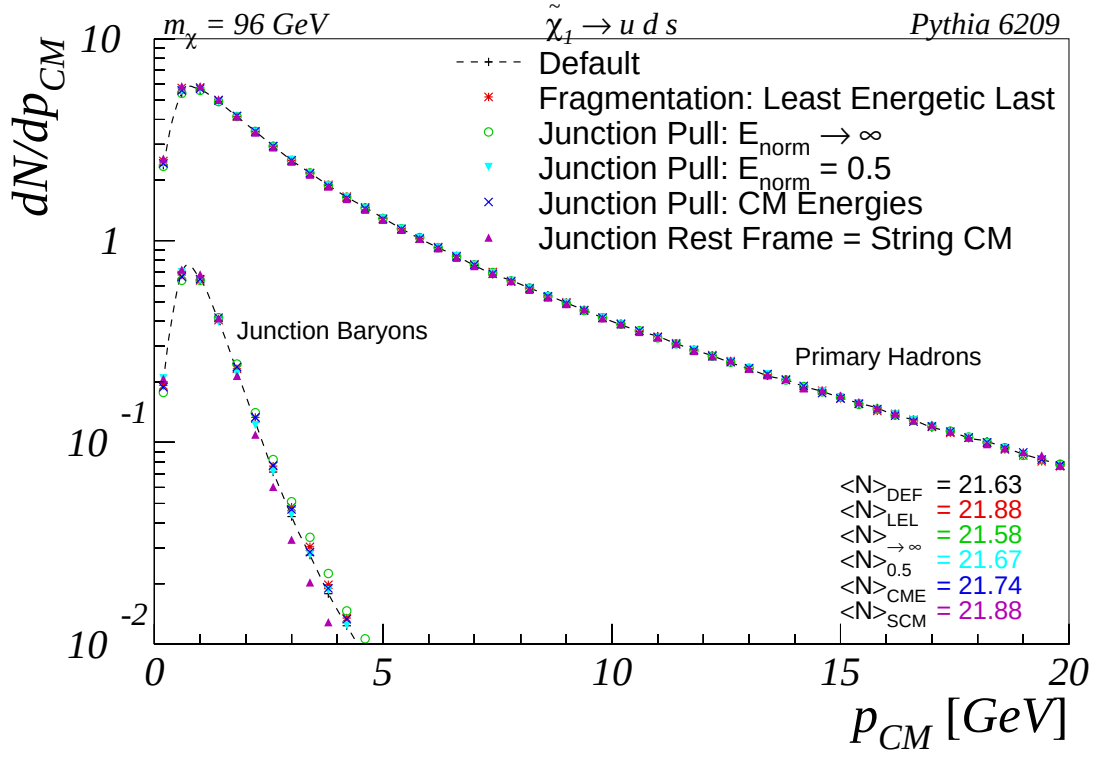

Figure 10: Momentum spectra of primary hadrons in the decays of a 96 GeV neutralino. Results with the default implementation are compared with five alternative ones. Average multiplicities of primary hadrons are shown in the lower right corner of the plot.

2. Replaced eq. (13), defining the junction pull vectors used in determining the junction rest frame, by a linear sum of 4-momenta instead of the default exponentially weighted sum, equivalent to setting $E_{\rm norm} \to \infty$ in eq. (13).
3. Enhanced the significance of soft gluon emission by setting $E_{\rm norm} = 0.5$ GeV rather than the default $E_{\rm norm} = 1.5$ GeV.
4. Switched off the iterative procedure for finding the junction rest frame, so that the energies appearing in eq. (13) are the string system CM energies rather than the energies in the junction rest frame.
5. Performed the fragmentation in the string system CM rather than in the junction rest frame.

The impact of these variations on the hadronization spectrum of a 96 GeV neutralino decaying to light quarks is shown in Fig. 10, where the rates of primary hadrons and junction baryons produced in the fragmentation are plotted as functions of their momenta in the CM of the decaying neutralino. Average hadronic multiplicities are shown at the lower right of the plot. As is readily observed, none of these variations lead to a significant change in the spectra; hence we believe the systematic uncertainties associated with these assumptions to be negligible to a good precision.

As a final variation, in Fig. 10 we also study what happens if the junction is assumed to be at rest in the string system CM frame (which agrees with the neutralino CM, unless a $g \to q\overline{q}$ splitting occurred in the shower). This is not intended as a realistic model variation, but indicates that even such extreme scenarios would not change the

qualitative picture of a low-momentum baryon. Here, however, we are helped by the fact that the three jets in the neutralino decay tend to be rather well separated in angle and that therefore the boost between the junction rest frame and the neutralino CM frame is not so large. Nevertheless, the more correct description gives a somewhat harder junction baryon spectrum, as should be expected from the boost.

5.2 Shower and hadronization activity

In section 3 we described the strategy for the generation of additional gluon radiation in BNV decays. Thereby the number of reconstructed jets can exceed the primary parton multiplicity. For our studies here we rely on the Durham jet algorithm [37], with a distance measure $y_{ij} = 2\min(E_i^2, E_j^2)\,(1-\cos\theta_{ij})/E_{\rm vis}^2$ between two particles or clusters i and j. Results can depend on the algorithm used, but we expect most of the phenomenology to come out similarly also for other algorithms [38].

In Fig. 11, jet rates are shown as functions of the $y_{\rm D}$ jet resolution parameter, with the jet clustering being performed in the center of mass of the decaying neutralino. The plots show a comparison between neutralino decay to light quarks (full lines) and neutralino decay to heavy quarks (dashed lines) for PYTHIA, at three stages of the event generation; (a) initial decay, (b) after parton shower, and (c) after hadronization.

In the initial decay, phase space is isotropically populated, and so no significant mass differences should be expected. However, since y_{ij} contains energies rather than e.g. momenta in the numerator, and since massive partons are assured nonvanishing energies, there are slightly more 3-jets for decays to heavy quarks. When the parton showers are included (cf. Fig. 11b), the suppression of gluon radiation off massive quarks ensures that decays into light quarks gives the larger number of further jets. Finally, hadronization (cf. Fig. 11c) once again flips the picture, at small resolution scales $y_{\rm D}$, mainly by the larger $p_\perp$ kick impaired to hadrons in the B meson decays. Such gluon radiation and hadronization effects are familiar from studies e.g. at LEP [15].

In comparing with theHERWIG implementation, we now concentrate on decays to light quarks so as to obviate the further complication of extra jets from heavy quark decays. This means that there are three main stages we can check for differences: 1) the population of the initial 3-body phase space, 2) the parton showers, and 3) the hadronization.

1. Phase space population. As mentioned above, PYTHIA produces an isotropic phase space population whereas HERWIG uses full matrix element weighting. In Fig. 12a a comparison of the jet rates between PYTHIA (full lines) and HERWIG (dashed lines) is shown for neutralino decay to light quarks. Only the three primary decay products are used in the jet clustering here. One notes that HERWIG has more 3-jets than PYTHIA over the whole $y_{\rm D}$ range. This agrees with expectations that the matrix elements should disfavour 2-jet configurations: in the 2-jet limit one invariant mass vanishes, meaning that contributions from graphs with that particular intermediate squark propagator also vanish. (A decay like $\tilde{\chi}^0 \to$ uds receives contributions from the three intermediate states $u\tilde{u}^*$, $d\tilde{d}^*$, and $s\tilde{s}^*$.) There are no squark poles in or near the phase space, however, so the variation of the matrix elements is rather mild. Thus effects of the matrix-element weighting are significant, but not dramatic.
2. Showering. In Fig. 12b we show the jet rates after showering but before hadronization. (For HERWIG this also means before the nonperturbative $g \to q\overline{q}$ branchings.) The difference produced in the initial decay is reduced slightly, but otherwise the pattern at high $y_{\rm D}$ is the same as above, with HERWIG producing more jets than PYTHIA. However, when the four-or-more jet rates come into play at lower val-

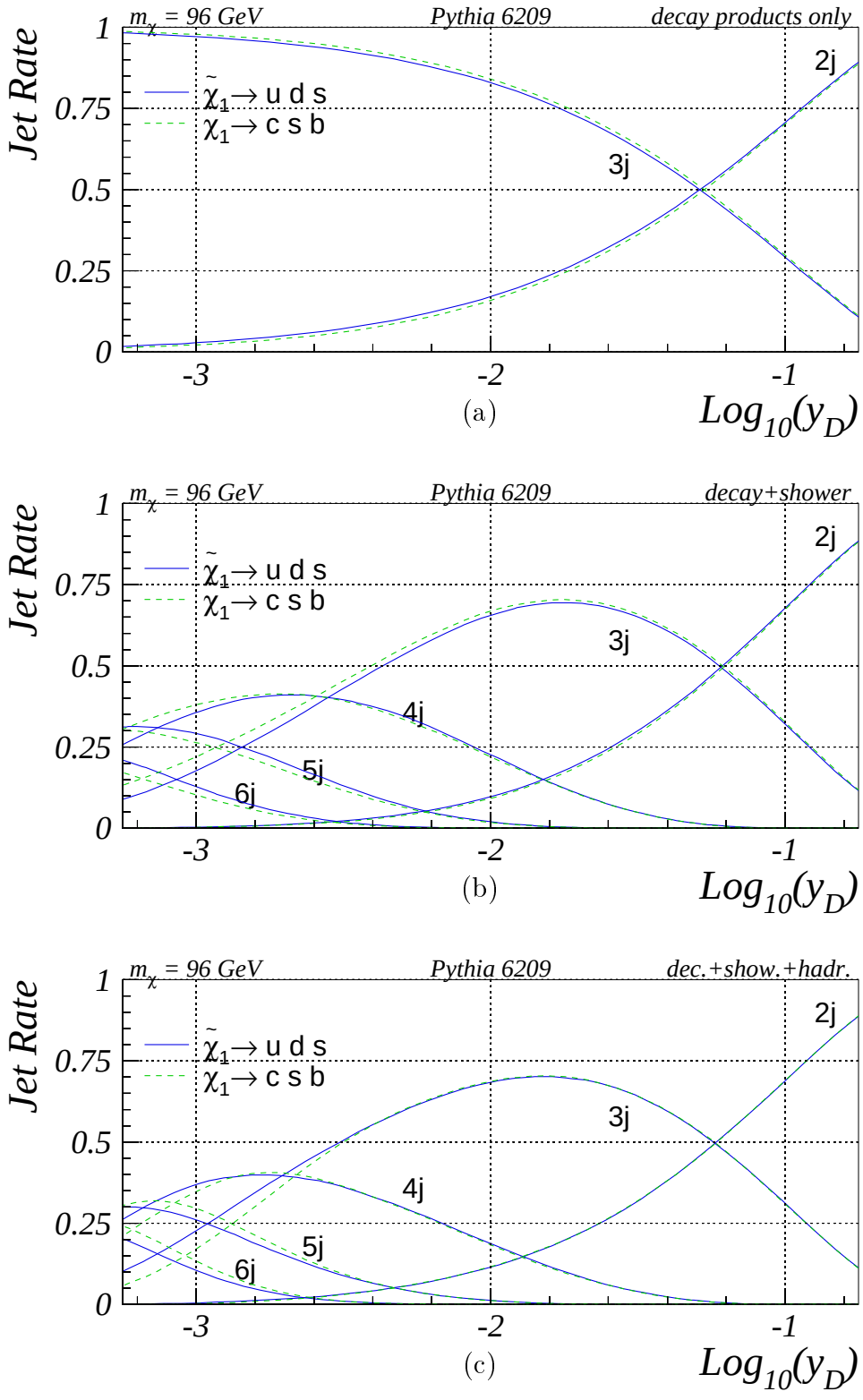

Figure 11: Jet rates in the decay of a 96 GeV neutralino resonance, $\tilde{\chi}^0 \to \mathrm{u}_i\mathrm{d}_j\mathrm{d}_k$, as functions of y_{D}. $\tilde{\chi}^0 \to$ uds is shown with full lines and $\tilde{\chi}^0 \to$ csb with dashed. (a) Clustering only of the primary neutralino decay products, (b) clustering after showering but before hadronization, and (c) clustering after full event generation.

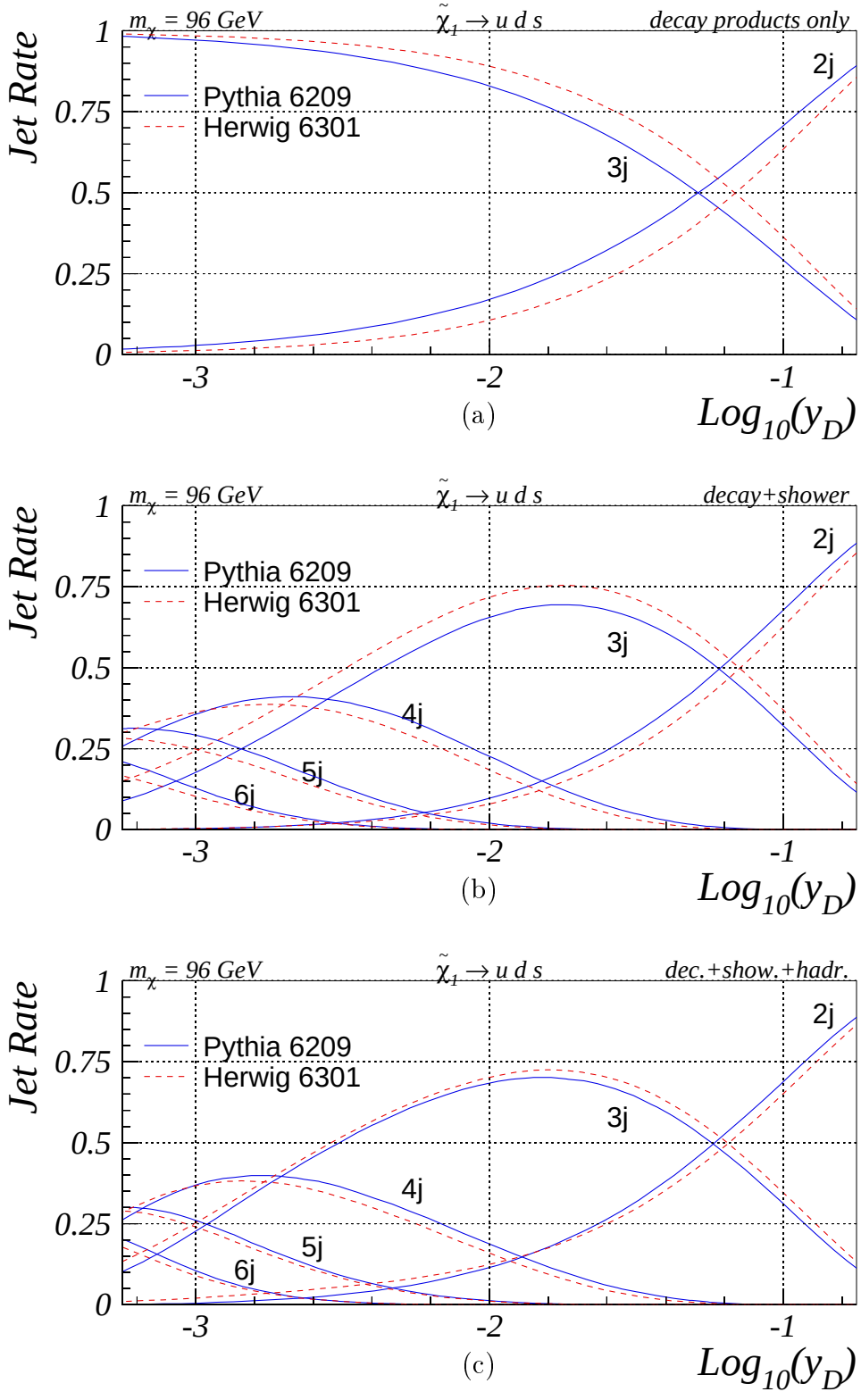

Figure 12: Jet rates in the decay of a 96 GeV neutralino resonance, $\tilde{\chi}^0 \to$ uds, as functions of y_D, as obtained with PYTHIA (full lines) and HERWIG (dashed lines). (a) Clustering only of the primary decay products, (b) clustering after showering but before hadronization, and (c) clustering of the final event.

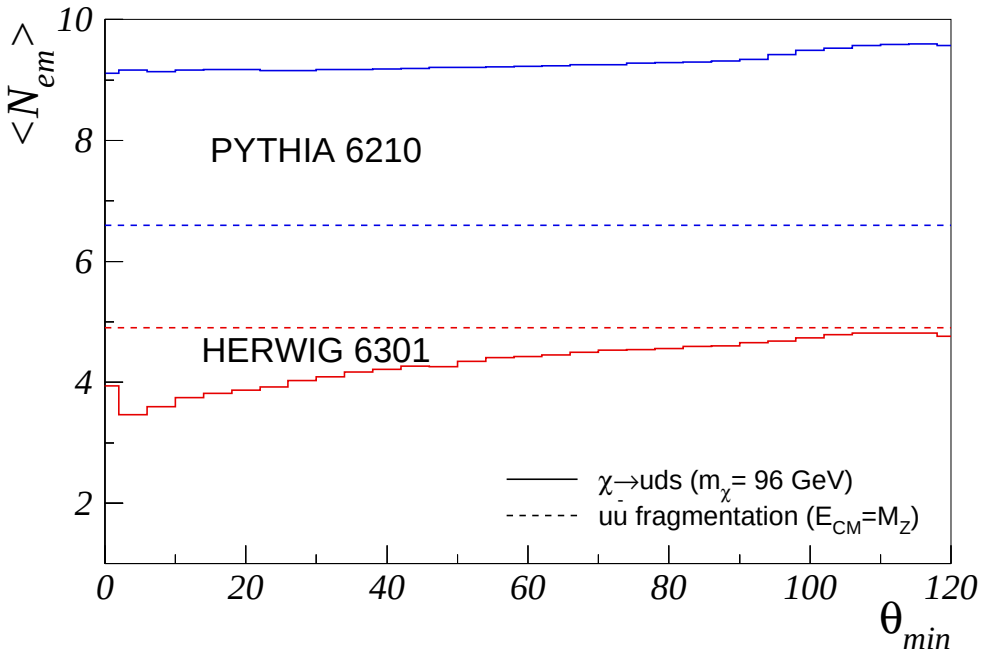

Figure 13: The average number of partons emitted in the shower of $\tilde{\chi} \to$ uds decays, as a function of the smallest opening angle between the neutralino decay daughters (solid lines; upper: PYTHIA, lower: HERWIG). The average number of partons emitted in $u\overline{u}$ cascades at the Z^0 resonance is shown for comparison (dashed lines).

ues of y_D, PYTHIA tends to produce more jets than HERWIG, even if there is still qualitative agreement.

We explore this difference by considering the number of partons emitted in the respective shower, Fig. 13. The variation from two- to three-jetlike topologies is characterized by the minimum opening angle between any two of the three original partons. Differences in the shower algorithms, such as the choice of cutoff scale, imply that the number of partons as such is not so informative. Therefore a convenient reference is offered by the respective results for ordinary $Z^0 \to q\overline{q}$ events, at a comparable energy.

In PYTHIA, the $\tilde{\chi}$ decays produce almost a factor 3/2 more radiated partons than does the Z^0 ones. This is consistent with a rather constant rate per radiating parton, somewhat reduced by the lower energy per parton in the $\tilde{\chi}$ decays. Such a result is not unreasonable, given that most gluons are emitted in the collinear regions around the quark directions, according to a universal radiation pattern, i.e. independently of the colour flow to other quarks at wide angles. One should note that the basic parton shower formalism of PYTHIA tends somewhat to overestimate energetic wide-angle emission in $Z^0 \to q\overline{q}$ events. This is then compensated by a rejection factor that reduces this emission to what is expected from the $q\overline{q}g$ matrix elements [18, 19]. Since no corresponding matching is implemented for $\tilde{\chi} \to qqq$ decays, it is quite likely that the shower activity here is somewhat overestimated. Further, in the limit that two partons become collinear, one should expect them partly to screen each other and the overall activity thereby to drop down towards the Z^0 level. That this does not happen in PYTHIA is an obvious shortcoming of the modelling, which is not set up to handle these screening effects.

By contrast, in HERWIG the variation with event topology is more marked: the

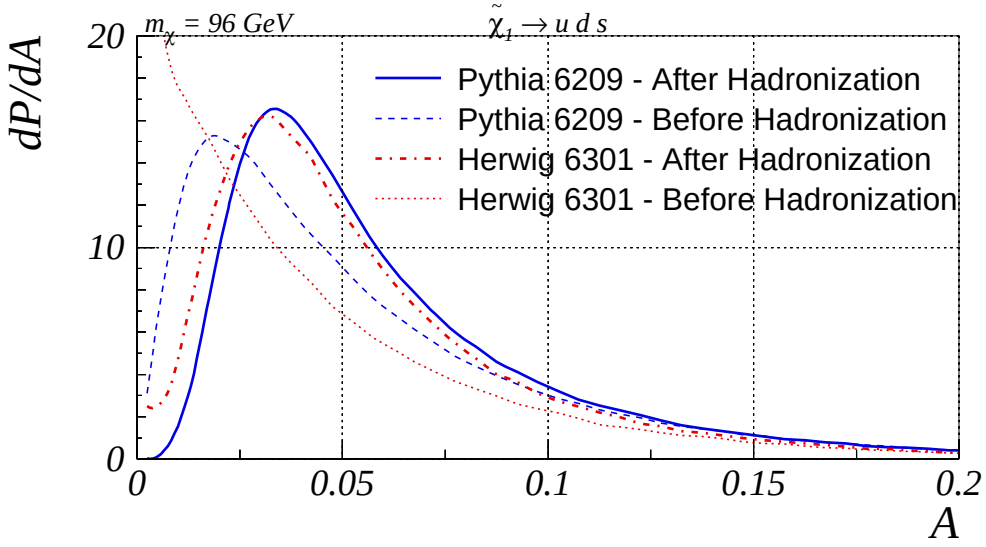

Figure 14: Distribution of linear Aplanarity, comparing PYTHIA and HERWIG.

HERWIG radiation cone is defined by the opening angle to one of the other quarks picked at random [8], meaning that two nearby partons may kill the radiation from each other. The most notable feature, however, is that the $\tilde{\chi}$ multiplicity is lower than the Z^0 one, also for well separated quark topologies, contrary to the arguments above.

We do not claim to understand the low emission rate in HERWIG. One observation, that we will quantify below, is that $\tilde{\chi}$ decays tend to have a large-mass central cluster, which could indicate a shortfall of emissions at wider angles. Among several potential differences between the two shower descriptions, it is then tempting to suspect the procedures used to start up the showers from some maximum virtuality. As we have already noted, the "dead zone" phenomenon is a well-known reason for HERWIG to underestimate multi-jet rates. If so, the differences should be larger for out-of-the-event-plane distributions than for inclusive ones, since the direction at 90° to the event plane is as far away as one can be from any of the three original quark directions. In Fig. 14, distributions of the linearized Aplanarity event shape variable [39] are compared. The curves relevant for showering are the dashed for PYTHIA and dotted for HERWIG. One observes that, also in the present case, HERWIG generates less activity out of the event plane than does PYTHIA. The steep rise of the HERWIG curve towards small Aplanarities is caused by events where no emissions harder than roughly 1 GeV or so occurred. The pattern is consistent with the hypothesis of a shortfall of wide-angle emissions in HERWIG.

3. Hadronization. The results of jet clustering after full event generation are shown in Fig. 12c. One notes that HERWIG still produces more jets at high y_D, whereas PYTHIA has more jets at small y_D, but overall the agreement between the two programs here is impressively and unexpectedly good. In particular, the hadron-level jet rate in HERWIG goes up appreciably relative to the parton-level one, whereas there is less difference between the two in PYTHIA.

   Of special relevance here is the HERWIG treatment of the "baryon cluster" which carries the net baryon number generated by the BNV decay. As we see from Fig. 15, this cluster has a rather different mass spectrum than other clusters, with a much higher average mass. (This is also noted in [8].) Such a large-mass cluster is first

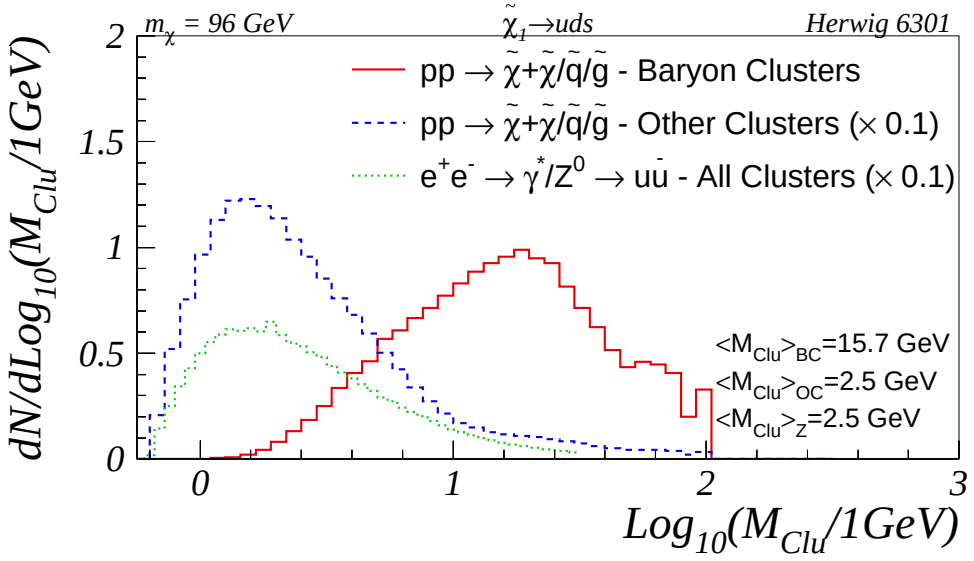

Figure 15: Herwig cluster mass spectra for the clusters containing non-zero baryon number (solid lines) as compared to the ordinary clusters from the neutralinos and the additional perturbative activity in the event. For reference, the cluster spectrum for hadronic Z^0 decays at 90 GeV are also shown (dotted lines). Only the baryon cluster spectrum is shown with its true normalization, the two other spectra having been normalized by a factor 1/10 to fit them onto the same scale as the baryon clusters.

fragmented into smaller clusters, which each then decay to hadrons. The fragmentation is along an assumed "string" direction, as appropriate for simple $q\overline{q}$ clusters. In the current case, where three leftover quarks are to be considered, two of these, picked at random, are combined to a diquark. The resulting system is fragmented along a single quark–diquark axis. The extreme case is those events, roughly 2% of the total number, where the whole neutralino becomes a single cluster. Then, as shown in Fig. 16, no well-separated third jet exists after hadronization, this information having been erased by the cluster formation procedure! In a normal event, effects tend in the opposite direction: some clusters appear along each of the three quark directions as a consequence of the shower activity, but then the baryon cluster also emits particles in a new "jet" direction intermediate to the two quarks that get combined into a diquark. The net result is an increase in the nonperturbative jet rate relative to the perturbative one. To the extent that this effect is unintentional, the large hadronization correction in Herwig is misleading.

To summarize, we note that the final agreement in jet rates must largely be viewed as coincidental, since all three contributing physics components by themselves differ between Herwig and Pythia.

5.3 The junction baryon

As discussed in subsection 4.4, the non-perturbative collapse of the colour wavefunction, which in our model results in a Y-shaped string topology, essentially "traps" the baryon number around the locus of the string junction. Thus, in the rest frame of the junction, we expect junction baryon momenta of the order of the hadronization scale. For well-separated jets, we further expect the junction rest frame to be only slightly different from

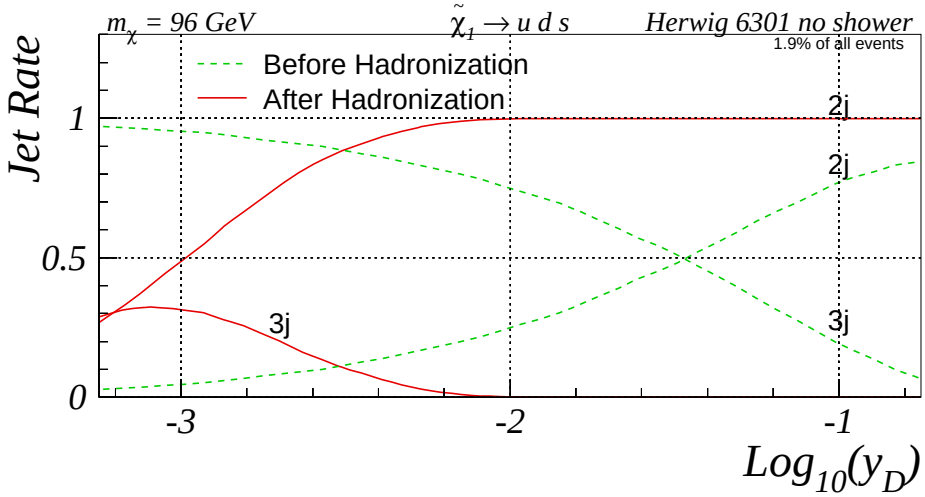

Figure 16: 2- and 3-jet rates before and after hadronization for HERWIG events with no gluon emission ($\sim 2\%$ of the event rate for default HERWIG).

the CM frame of the decay. Thus a generic feature of our model is the prediction that the baryon number generated by BNV decays predominantly ends up in baryons which have small momenta relative to the decaying particle.

In Fig. 17 the rates of both junction baryons and "ordinary" baryons are plotted as functions of their CM momenta for $\tilde{\chi} \to$ uds for (a) two different neutralino masses (Snowmass points 1a and 1b), and (b) comparison between PYTHIA and HERWIG for a 96 GeV neutralino.

As expected, one observes a much sharper peaking towards low momenta for the junction baryon distributions as compared to the ordinary baryon distributions in Fig. 17a. Also, note that this peaking does not depend on whether the neutralino is light or heavy. A heavier neutralino gives rise to longer strings, i.e. larger momenta and higher multiplicities, as can be seen by the shift in shape and normalization of the ordinary baryon momentum distribution, but this does not significantly affect how much energy will eventually be available to form the junction baryon. The slight hardening of the junction baryon momentum for a higher neutralino mass is attributable to the increased phase space for perturbative gluon emission, which gives the junction a slightly higher average velocity in the neutralino rest frame.

In Fig. 17b we compare with the HERWIG implementation. Of course, HERWIG does not have junctions and so no junction baryons *per se*, but it is nonetheless possible in most cases to trace the BNV-associated baryon number, via a cluster with non-vanishing baryon number, to a specific final-state baryon. And so, with a slight abuse of nomenclature, we term this baryon the HERWIG "junction baryon". Naturally, both programs produce only one junction baryon per decay. However, as shown in Fig. 17b, the HERWIG fragmentation produces 1.1 ordinary baryons more, on the average, than does PYTHIA. Interpreted as a systematic uncertainty on the baryon multiplicity in fragmentation, this difference is disturbingly large. However, when comparing with the LEP experimental value at the Z^0 peak, $\langle n_{\rm p} \rangle_{\rm LEP} = 0.98 \pm 0.1$ [15] protons per event (neutrons not being measured), default PYTHIA with its 1.2 protons per event comes closer than default HERWIG with its 1.5. Presumably a better tuning to LEP than offered by the defaults would also reduce the difference seen in neutralino decays.

The difference in the description of the junction baryon should persist, however.

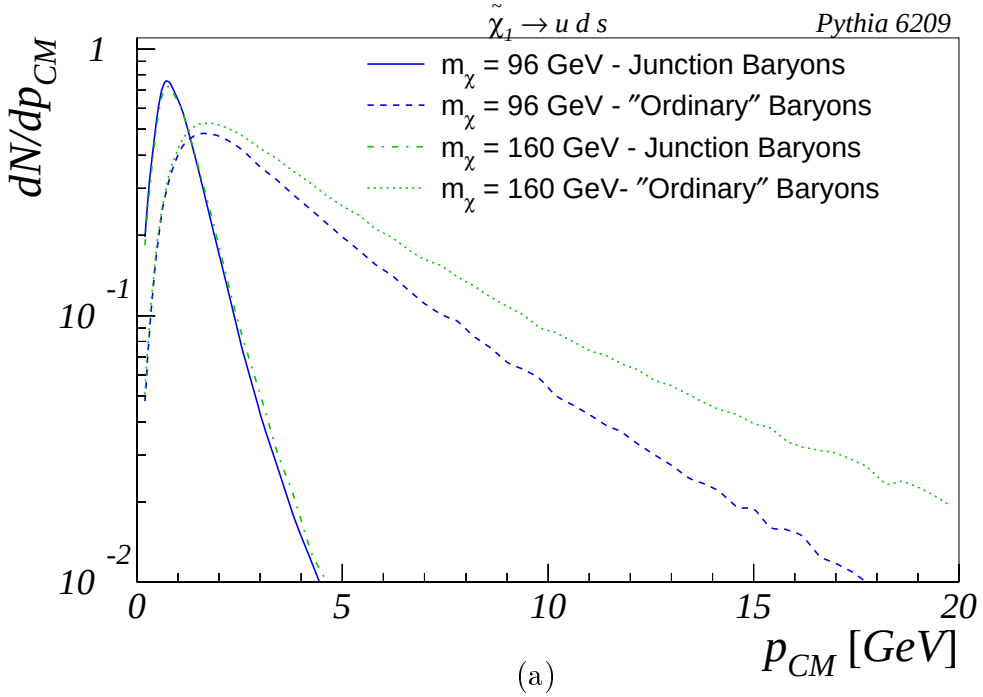

(a)

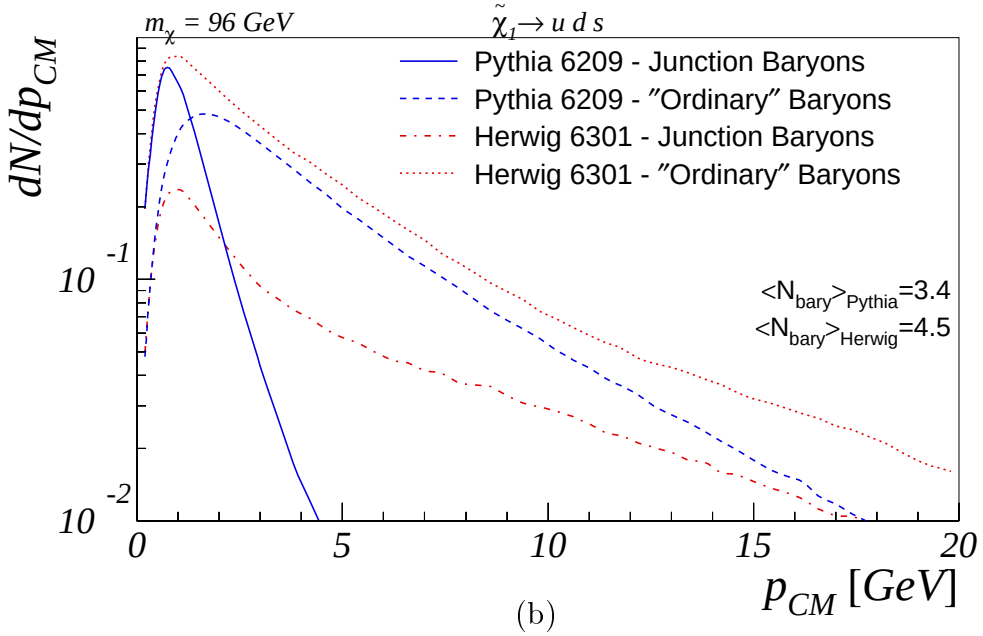

(b)

Figure 17: CM momentum distributions in the decay of a 96 GeV neutralino for junction (full line) and ordinary (dashed line) baryons (a) as compared to the decay of a heavier neutralino (dot dashed and dotted line for junction and ordinary baryons respectively), and (b) as compared to the same process in HERWIG (dot dashed and dotted line for junction and ordinary baryons respectively).

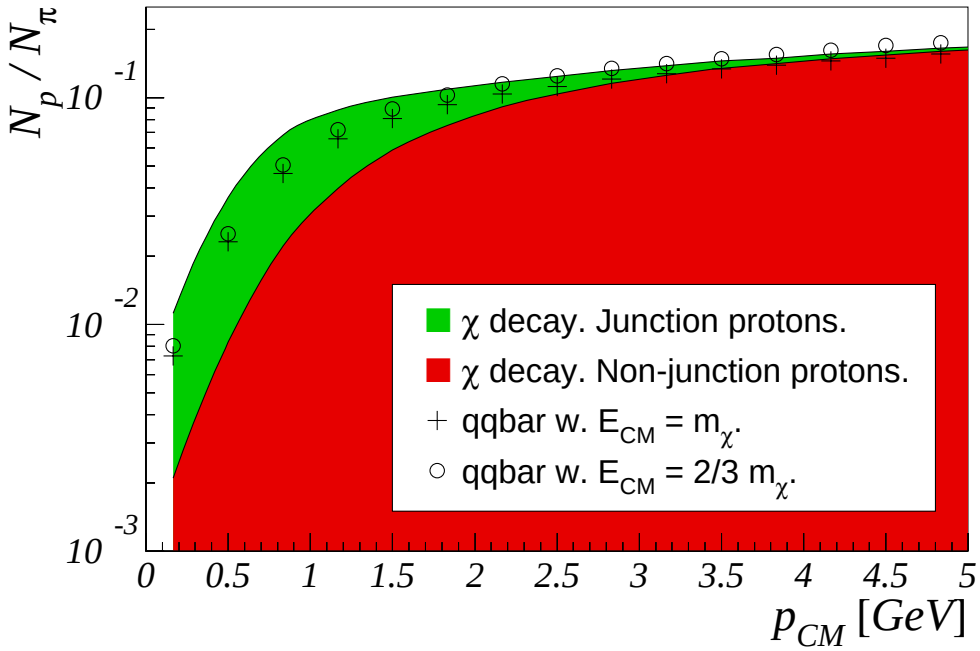

Figure 18: Proton (+antiproton) CM-frame momentum spectrum normalized to the charged pion one. Distributions are shown for 96 GeV neutralino decays to light quarks (junction and non-junction proton contributions shown separately) and for two cases of ordinary $q\overline{q}$ fragmentation, one (crosses) where the total CM energy is the neutralino mass and one (circles) where it is only $\frac{2}{3}m_{\tilde{\chi}}$, in order to make the energies of each piece of string equal.

In Herwig there is no particular reason why this baryon should be slower than other baryons, and this results in a distribution for junction baryons which looks more or less the same as that for ordinary baryons, a situation quite at contrast to the shape of the junction baryon spectrum predicted by the model presented here, cf. Fig. 17b. This means that the Herwig model offers less hope to find direct evidence for the occurrence of BNV. We believe, however, that this model is unrealistic, being flawed by an underestimated shower activity in combination with an unphysical description of the fragmentation of the baryon cluster, as explained above in section 5.2.

When comparing baryon rates between physical processes, differences in the overall multiplicity may confuse the issue. For instance, a $\tilde{\chi} \to qqq$ decay should have a larger multiplicity and softer fragmentation spectra than a $\gamma^*/Z^* \to q\overline{q}$ decay of the same mass, since the total energy is shared between more strings. A decay to two gluons, such as $h^0 \to gg$, would have an even larger multiplicity, owing to the gluon energy being shared between two strings and, by the same colour charge argument, also radiating more in the perturbative phase. A more realistic measure is the fraction of (anti)protons among charged particles, where the issue of overall multiplicity divides out, and quark and gluon jets of different energies give almost identical results at low momenta. In Fig. 18 we show the ratio of proton to pion momentum spectra, which is basically equivalent with the above. (Inclusion of kaons along with the pions would not affect the relative difference between scenarios.) The mass differences and decay patterns give a softer pion than proton spectrum, and therefore a rising p/π ratio. In the neutralino decay, the significant

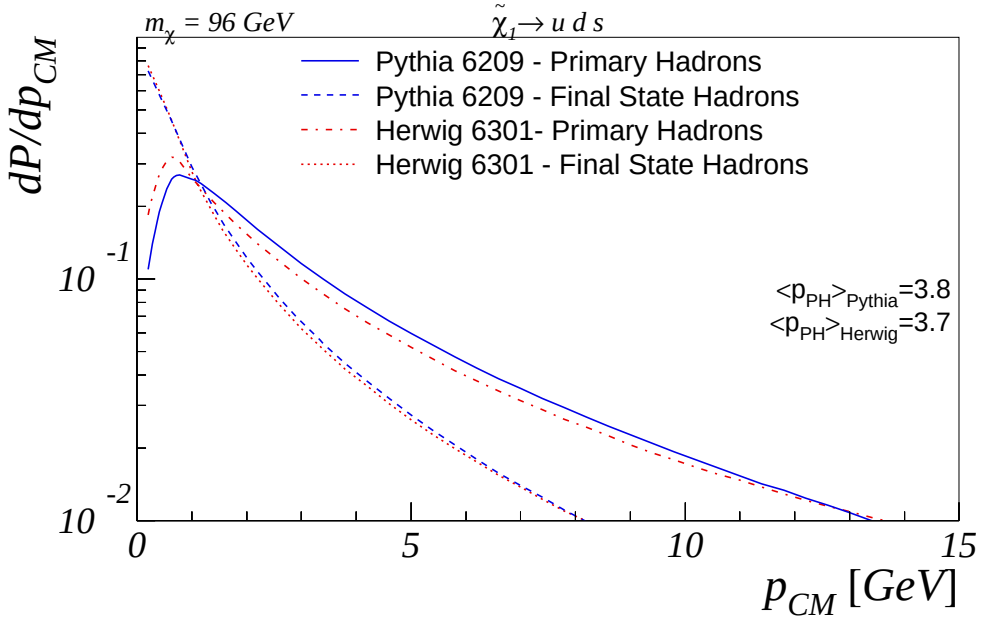

Figure 19: CM momentum distributions in the decay of a 96 GeV neutralino for primary hadrons (PYTHIA full lines, HERWIG dot-dashed) and final state hadrons (PYTHIA dashed lines, HERWIG dotted). At the bottom left, the mean primary hadron momenta are shown for each of the two programs.

enhancement caused by the junction baryon contribution is again visible. It is noteworthy that the case of a $q\overline{q}$ (or gg) decay gives a ratio intermediate to the ones in the qqq decay without and with the junction baryon included. The explanation is that the low-momentum region in the qqq topology is depleted from normal baryon production by the presence of the junction baryon. Unfortunately, this means experimental signals are not quite as dramatic as might have been wished for, as we shall see.

5.4 Generic event properties

We now turn our attention to a comparison of the expected overall event features between PYTHIA and HERWIG, specifically as characterized by the fragmentation spectra and the multiplicity distributions for charged hadrons.

In Fig. 19 we show the hadronic fragmentation spectra produced by the decay $\tilde{\chi} \rightarrow$ uds. With "primary hadrons" and "final state hadrons" we understand hadrons produced in the fragmentation of the strings, before and after decays take place, respectively. There is good agreement, with slightly smaller primary hadron momenta being produced by HERWIG as compared to PYTHIA.

In Fig. 20 is compared the multiplicities of charged hadrons as produced by PYTHIA and HERWIG. An average difference of almost 2 charged hadrons can be observed. When performing the same comparison for the LEP1 process $e^+e^- \rightarrow$ hadrons, where $\langle n_{ch} \rangle_{\rm LEP} = 20.92 \pm 0.24$ [15], the PYTHIA 21.0 and HERWIG 20.1 values also differ. This mistuning partly explains the difference for neutralino decay between the two programs. One should remember that the two hadronization models for this kind of configurations are quite different from the respective description of Z^0 decay, however, so there is no strong reason for the two programs to agree, neither with each other nor with the Z^0 numbers.

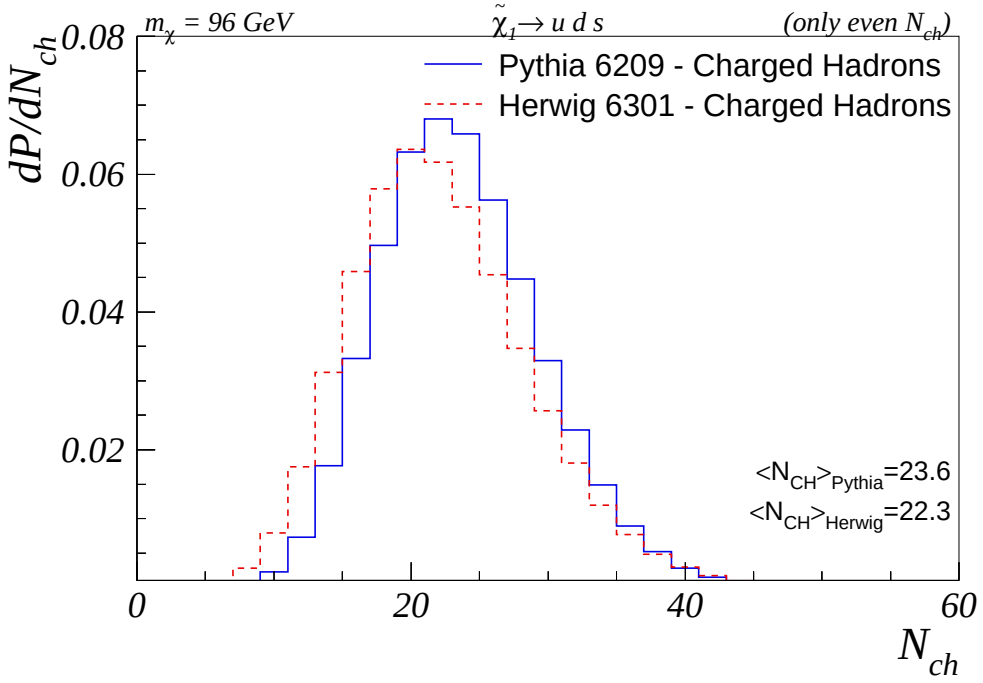

Figure 20: Charged hadron multiplicities in the decay of a 96 GeV neutralino as obtained with PYTHIA (full lines) and HERWIG (dashed). At the bottom left, the mean charged hadron multiplicities are shown for each of the two programs.

Consider e.g. the simple string model, which predicts a logarithmic increase of the multiplicity with jet energy, $\langle n \rangle \propto \log(E/m_0)$, where m_0 is some typical hadronic mass scale of order 1 GeV. Taking LEP events to consist of two jets with half the energy each, and neutralino decays to be three jets with a third each, the above LEP1 multiplicity would translate into something like 28 charged particles per neutralino decay. That the programs predict multiplicities much below this indicates the importance of the details of the event description.

5.5 Alternative string topologies

Until now, we have considered only neutralino decay, since most of the salient features of our model stand out more clearly in this case. Nevertheless, in regions of SUSY parameter space where the BNV couplings are either larger than the gauge couplings, or where the gauge decays of the lowest-lying squark mass eigenstate are kinematically suppressed or forbidden, a special situation arises: the direct 2-body BNV decays listed in section 2 dominate for the lowest-lying squark mass eigenstate. This gives us a unique chance to study the more exotic string topologies discussed in section 4.5: junction–junction strings and junction–junction annihilation.

To quantify, we here take a generic "light stop" SUSY spectrum, Snowmass point 5, with $m_{\tilde{t}_1} = 220$ GeV, and the decay $\tilde{t}_1 \rightarrow \tilde{\chi}_1^+ b$ kinematically inaccessible. Since we wish specifically to study 2-junction and 0-junction topologies, we assume third generation BNV couplings of order 0.1 or larger, so that the stop lifetime, cf. eq. (14), is sufficiently small that string breaks between the stops will not normally occur before decay. Furthermore, we require that the stops be produced in an overall colour-singlet state, so

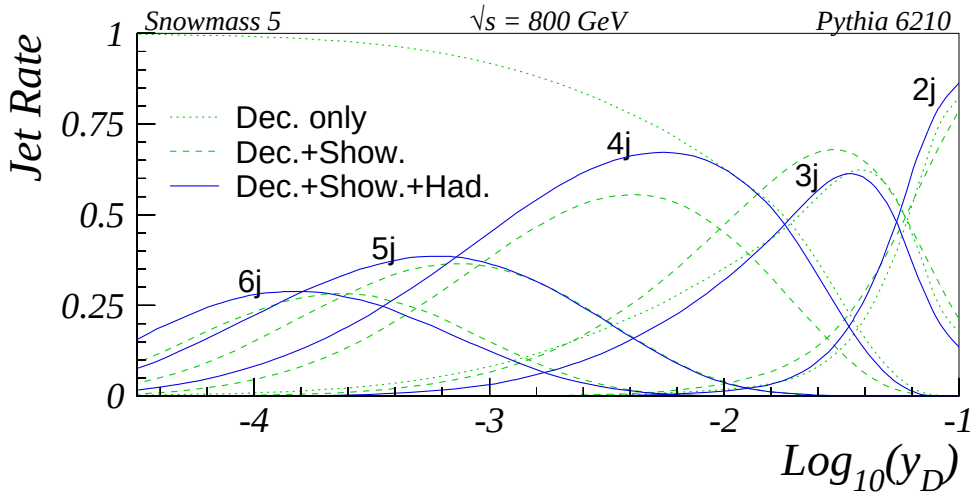

Figure 21: Jet rates for the process $e^+e^- \to \tilde{t}_1(\to \bar{d}\bar{s})\tilde{t}_1^*(\to ds)$ at 800 GeV CM energy, as functions of y_D, for three stages of the event generation: clustering only of the primary $\tilde{t}_1\tilde{t}_1^*$ decay products (dotted curves), clustering after showering but before hadronization (dashed curves), and clustering after full event generation (solid curves).

that their decays, leaving out the possibility of colour reconnections in the final state, are colour-connected to each other. This will generally not be the case at hadron colliders since, in processes like $gg \to \tilde{t}_1\tilde{t}_1^*$, each stop inherits its colour from a parton in the initial state rather than from the other stop.

Consequently, we consider the process $e^+e^- \to \tilde{t}_1\tilde{t}_1^*$, with the stops decaying to light quarks, $\tilde{t}_1 \to \bar{d}\bar{s}$. Again, differences with respect to the HERWIG implementation exist, but since we expect the main part of these to be covered already by the discussion in the preceding subsection, we do not perform explicit comparisons here. Suffice it to note that the hadronization model for BNV squark decays adopted in HERWIG roughly parallels that of PYTHIA with only 0-junction configurations.

As was observed in subsection 4.5, the probability for two connected junctions to annihilate is almost unity close to threshold in our model. To ensure that the case where we let the choice between a 0-junction and a 2-junction topology be determined dynamically, i.e. by eqs. (20)–(23), indeed does differ from the pure 0-junction case, we choose a CM energy somewhat above threshold. For Snowmass point 5, the threshold is $2m_{\tilde{t}_1} = 440$ GeV, thus a CM energy of 800 GeV is appropriate. This results in a junction–junction annihilation rate of about 0.6, cf. Fig. 8.

We again begin by considering the jet rates, for the specific process $e^+e^- \to \tilde{t}_1(\to \bar{d}\bar{s})\tilde{t}_1^*(\to ds)$ at 800 GeV CM energy. The jet clustering is performed using a Durham algorithm in the e^+e^- CM frame, yet since we here make the simplification of neglecting initial-state radiation and beamstrahlung, this frame is identical to the $\tilde{t}_1\tilde{t}_1^*$ CM. Note that this frame need not generally coincide with the $\tilde{t}_1\tilde{t}_1^*$ CM at decay time, due to the possibility of the stop pair emitting final-state radiation.

In Fig. 21 we show the jet rates for dynamical selection between 2-junction and 0-junction topologies, as functions of y_D. To trace the evolution of the event, we plot the rates for initial decay (dotted curves), after parton shower (dashed curves), and after hadronization (solid curves).

Since each stop decays to a 2-body final state, we obtain four jets at leading order. As

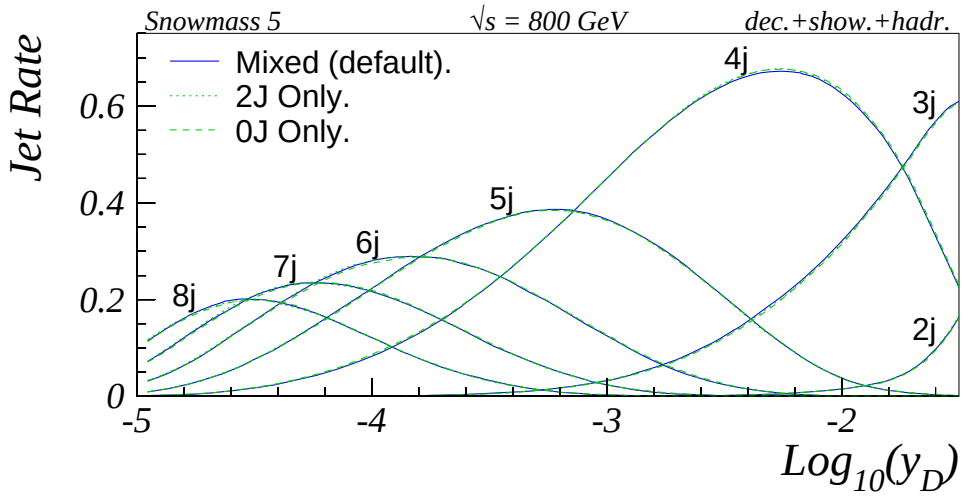

Figure 22: Jet rates for the process $e^+e^- \to \tilde{t}_1(\to \bar{d}\bar{s})\tilde{t}_1^*(\to ds)$ at 800 GeV CM energy, as functions of y_D, for three choices of string topology: mixed 0-junction and 2-junction (solid curves), 2-junction only (dotted curves), and 0-junction only (dashed curves).

can be observed from the dotted curves in Fig. 21, the initial decay daughters are actually clustered to fewer than 4 jets for a non-negligible fraction of the events down to quite low values of y_D, this due to asymmetric decays causing two daughters to end up close to each other and so be clustered to one jet rather than two.

The question now arises to what extent, if any, the choice of string topology affects the jet rates. To study this, in Fig. 22 we replot the solid curves of Fig. 21 together with the two extreme cases where all events are forced to be either of the 2-junction (dotted curves) or the 0-junction (dashed) type. Note that the latter sample has a small contamination of 2-junction events, from perturbative breakups in the $\tilde{t}_1\tilde{t}_1^*$ shower. As can readily be observed, the curves are identical to a high precision, bearing witness to the absence of any resolvable structural difference between the topologies, at least for the y_D ranges and jet numbers we found it meaningful to include in the analysis.

We thus do not believe that these semi-inclusive observables could be used e.g. to measure the junction–junction annihilation rate. We return to the issue of whether exclusive quantities can do a better job in the more experimentally oriented study in subsection 6.3.

6 Experimental tests

In this section we present some semi-realistic studies on how baryon number violation could be pinned down experimentally. We do not propose to recapitulate the extensive experience on SUSY search strategies, with likelihood techniques or a succession of cuts and sideband subtraction procedures, required to isolate signals relative to backgrounds for different SUSY parameter sets. Rather, we assume that a signal has already been found in multijet final states, with bumps in the two- or three-jet invariant mass distributions consistent with the presence of new particles. The key issue is then whether this is evidence for SUSY with BNV or for some completely other physics signal. The decision is likely to be based on a combination of different pieces of information, but a crucial

one would be to find the baryon associated with the BNV itself. This is not possible on an event-by-event basis, owing to the background of normal baryon production and the non-identification of neutrons. What we can aim for is then to demonstrate the existence of a statistically significant excess (or not) of baryon production in the momentum region predicted by our model.

This kind of demonstration will most likely be beyond the reach of the Tevatron; therefore in the following we concentrate on an LHC scenario with pp collisions at $\sqrt{s} = 14$ TeV. We take a crude representation of the ATLAS tracking and calorimetry capabilities (described below) to be sufficiently detailed for the kind of analysis we will consider, specifically whether an excess of protons à la Fig. 18 can still be seen for fully generated events in a semi-realistic detector environment.

Of course, a similar exercise could have been performed for CMS but, at our level of detail, we expect the differences between the two experiments to be of negligible consequence. The exception would be baryon identification strategies, see below.

With respect to the prospects at linear colliders, the comparatively clean environment and high luminosity imply that studies similar to the ones presented here would be easier to carry out, although they would obviously have to wait for such a facility to be built. Therefore, we constrain our attention in this direction to one special case, that of colour-connected BNV $\tilde{\mathrm{t}}_1\tilde{\mathrm{t}}_1^*$ decays, which we expect to be nigh impossible to study with hadron colliders.

6.1 Detector layout and acceptance

Based primarily on the ATLAS physics TDR [40], we assume a calorimeter that covers the region $|\eta| < 5$ in pseudorapidity and $0 < \phi < 2\pi$ in azimuth, with a granularity of $\Delta\eta \times \Delta\phi = 0.1 \times 0.1$. This reproduces the expected ATLAS calorimeter granularity at mid-rapidity, but overestimates it at large rapidities. Smearing due to finite resolution effects has not been simulated.

Proton and pion reconstruction. For $\mathrm{p}^\pm$ and $\pi^\pm$ reconstruction and identification we use the region $|\eta| < 2$, well inside the coverage of the ATLAS and CMS tracker systems. Inside this region, all charged hadrons with $p_\perp > 1$ GeV are reconstructed. This is somewhat more optimistic than what would be possible in the real world. Particles with $p_\perp < 1$ GeV predominantly come from the underlying event, so the $p_\perp$ cut reduces the study to particles associated with the hard physics of the event.

Ideally, we would like to identify all charged hadrons in the above region, with complete separation between the $\mathrm{p}^\pm$ signal and the $\pi^\pm$ and $\mathrm{K}^\pm$ background. In reality this will never be possible. Neither ATLAS nor CMS has yet carried through detailed detector simulation of their proton identification performance. Our physics scenario may represent the first example where this capability is relevant in the study of physics beyond the Standard Model, and so could offer a convenient target for future detector studies. (QCD physics obviously provides several reasons to have this capability, one of which will be mentioned later.) In the meantime we exemplify what could be possible.

The conservative approach is to restrict the search to the $\Lambda^0 \to \mathrm{p}^+\pi^-$ channel which, due to its two charged tracks from a displaced vertex and narrow mass peak, offers a reasonably clean signal. This channel also has the advantage that it doesn't cut down the statistics much: the flavour composition of fragmentation in $\mathrm{e}^+\mathrm{e}^-$ annihilation is measured to give $N_{\Lambda^0}/N_\mathrm{p} \sim 0.4$ [41] and the branching ratio of Λ^0 to $\mathrm{p}^+\pi^-$ is about 60% [41], so about one in every four protons comes from a Λ^0 decay to $\mathrm{p}^+\pi^-$. Since the proton inherits

most of the momentum in the Λ^0 decay, the proton plots shown below would also apply for Λ^0, with minor modifications.

Nevertheless, one may aggressively assume some proton identification capability, to augment the statistics from the Λ^0 decay, and maybe also to clean up this signal from the $\mathrm{K}^0_\mathrm{S} \to \pi^+\pi^-$ background. For ATLAS, charged hadron identification is not a prime objective for the Inner Detector, but the ionization loss, $\mathrm{d}E/\mathrm{d}x$, in the Transition Radiation Tracker gives enough information to separate protons from pions by more than 1σ in the momentum range 3 GeV $\lesssim p \lesssim$ 20 GeV [40]. However, the $\mathrm{K}^\pm/\mathrm{p}^\pm$ separation is very poor even in this range, so an analysis purely based on this capability will contain a non-vanishing misidentification background. Calorimetry provides auxiliary information, especially for antiprotons, which release an additional GeV of energy by their annihilation. This should be noticeable, at least for antiprotons stopping in the electromagnetic calorimeter. For protons the mismatch between energy and momentum goes in the other direction and is smaller. We note that the hadrons discussed here are not ones found in the core of jets, and anyway have so low momenta that they are significantly deflected by the magnetic field. Therefore they are likely to be isolated in the calorimeter.

The possibility to use $\mathrm{d}E/\mathrm{d}x$ in the CMS silicon tracker is still under study, but in any case the tracker has only a few sampling points, and so limited capability in this respect. On the other hand, there is considerable empty space between the silicon layers. Therefore one can imagine to install a time-of-flight system at some future date. This would allow good proton identification in the lower part of the interesting momentum range. As above, calorimetry could be used to identify some of the antiprotons.

Jet reconstruction. We use a cone algorithm over the full fiducial volume of the calorimeter, $|\eta| < 5$, with a cone size of $\Delta R = \sqrt{\Delta\eta^2 + \Delta\phi^2} = 0.4$ and a minimum jet seed energy of 5 GeV. Reconstructed jets with a transverse energy below 25 GeV are not used in the further analysis. No jet energy recalibration procedure has been applied.

6.2 Physics cuts

As mentioned above, we assume that a relatively clean sample of SUSY events has been isolated before the present analysis is applied, hence we do not study SM backgrounds. The event sample thus consists of a general SUSY simulation for our reference point, Snowmass point 1a [36], including all SUSY processes currently implemented in Pythia. Most of these, however, are suppressed at hadron colliders so that the cross section is dominated by gluino and squark production. We concentrate on the case where the BNV couplings are smaller than the gauge couplings, thus sparticles will only use the BNV channels as a "last resort". That is, the ordinary MSSM pattern of cascade decays will persist, with the modification that the LSP decays. Assuming that the lightest neutralino is the LSP, we are thus looking at events of the type:

$$2(\mathrm{q/g}) \to 2(\tilde{\mathrm{q}}'/\tilde{\mathrm{g}}) \to 2(\mathrm{q}''/\mathrm{g})(+X) + 2(\tilde{\chi}^0_1) \to 2(\mathrm{q}''/\mathrm{g})(+X) + 2(\mathrm{q}_i\mathrm{q}_j\mathrm{q}_k), \qquad (24)$$

where the two initial partons come from the beam protons and X signifies what, if anything, is split off in the cascades besides the neutralinos. Since the neutralinos are not colour connected to the rest of the event, we note that this type of event is nothing but an ordinary R-conserving MSSM cascade event with the missing energy transformed into two separate $\tilde{\chi}^0_1$ decays.

For such events, about 25% of the junction protons lies within the detector acceptance. Without any further cuts, the equivalent of Fig. 18 looks as depicted in Fig. 23. A rather

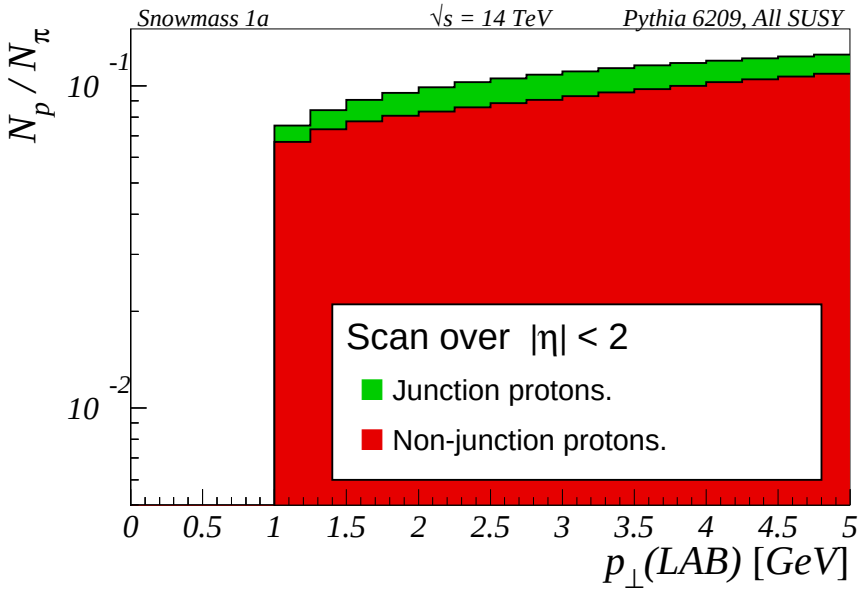

Figure 23: Reconstructed $p_\perp$ spectrum for the ratio of protons to charged pions in a simple scan over the detector volume.

depressing result, of course due to the many protons which originate exterior to the neutralino decay itself, and to the fact that we are looking at momenta in the CM of the original collision rather than in the CM of the neutralino.

However, it is possible to do much better by placing cuts designed to identify the 3 jets from each of the $\tilde{\chi}_1^0$ decays, reconstructing the presumed $\tilde{\chi}_1^0$ CM and looking for low-momentum protons in that frame. In principle, it would be even better to attempt to reconstruct the junction rest frame itself, based on the directions of the three jets. Here, we note that for well separated jets, as seen in the neutralino CM, the junction rest frame is at any rate closely approximated by the CM frame, and so in this preliminary study we content ourselves with working in the 3-jet CM.

We use two different strategies to identify the neutralino decay jets. The first, blind 3-jet reconstruction, probably does worse than what could be done with more elaborately designed cuts, and the second, optimized 3-jet reconstruction, probably errs on the side of too optimistic results. Thus, the actual experimental result should lie somewhere between these two extremes.

6.2.1 Blind 3-jet reconstruction

We term this analysis "blind" since we assume no *a priori* "divine knowledge" of which jets are the correct ones etc. Thus, we use a selection of cuts to attempt to identify the neutralino decay jets as precisely as possible, then reconstruct the presumed neutralino CM and look for low-momentum particles there. Since our cuts have not been through a long, rigourous optimization procedure, it is likely that we err on the low side of what could be done with better optimized cuts.

Note also that our cuts rely to some extent on features specific to the SUSY scenario we use (Snowmass point 1a), but they should produce acceptable results for any scenario that shares its general features: a neutralino LSP and a rather light sparticle spectrum

with a relatively large gap between the squarks (and the gluino) and the LSP.

With this type of spectrum, the squark/gluino decays release much kinetic energy, giving rise to generally high-$p_\perp$ neutralinos. Since the $\tilde{\chi}_1^0$ mass itself is small in comparison, its three decay jets always occupy a relatively small total region of the detector. These two considerations form the backbone of our cuts. In decays like $\tilde{\chi}_1^0 \to$ csb, one could furthermore require heavy-quark tagged jets, but we do not rely on such extra information here.

To quantify, we select events with 8 or more reconstructed jets and in those look for systems of 3 jets which have a total $p_\perp^{3\mathrm{j}} > 200$ GeV. The measure we use for how far the three jets are from each other in the detector is the maximal jet–jet R distance:

$$\Delta R_{\mathrm{jj}}^{\max} = \mathrm{Max}(\Delta R_{\mathrm{j_1 j_2}}, \Delta R_{\mathrm{j_2 j_3}}, \Delta R_{\mathrm{j_3 j_1}}) \tag{25}$$

where j_i stands for the i'th jet in the candidate 3-jet system. We impose a cut requiring $\Delta R_{\mathrm{jj}}^{\max} < 0.8$. Since we use a cone size of $\Delta R = 0.4$, this cut translates into looking for 3 jets which overlap or just touch each other. The details of how the energy in the overlapping regions is assigned to the each of the overlapping jets depends on the particular jet algorithm used. However, as long as double counting is avoided, we do not expect these details to influence our analysis; ideally, the CM of the 3 jets should be invariant to changes in the sharing of energy between its 3 constituent jets.

To further bring down the combinatorics, we require that none of the 2-jet pairs in the 3-jet configuration have an invariant mass close to or larger than the neutralino mass. Assuming that this is already known to some precision, we reject candidate 3-jet systems where any pair of jets has a mass larger than 90 GeV. Of the remaining candidate 3-jet systems, we select those which reconstruct to the neutralino mass ± 10 GeV.

For each of these 3-jet systems we search for candidate junction protons within the detector acceptance described above. We check whether there are any (anti)protons within $\Delta R_{\mathrm{p3j}} < 0.5$ of the 3-jet system momentum direction. Any such protons are accepted as candidate junction protons. About 5% of the junction protons within the detector acceptance survive these cuts. The corresponding number for the non-junction protons is 0.2%.

The interesting quantity now is the momenta of these protons in the 3-jet system CM frame, our first approximation of the junction rest frame. As has been argued above, we expect that the real junction protons will exhibit a softer momentum spectrum in this frame than will be the case for non-junction protons. Thus, we expect that the enrichment of the sample by junction protons should be largest for small proton momenta in the reconstructed neutralino CM. Results are depicted in Fig. 24.

The situation has improved noticeably over the one in Fig. 23, but there is still a lot of non-junction protons at small $p_\perp$ which, as we shall see in the next subsection, may be further reduced by reducing the combinatorial background, i.e. by having a more precise identification of the correct neutralino decay jets.

6.2.2 Optimized 3-jet reconstruction

We now assume that a nearly perfect neutralino decay jet identification can be performed, by applying some selection of cuts, the details of which are not interesting here. Rather, we mimic the effects of such optimized cuts by using the event generator information.

For each of the neutralino daughters, we select that jet which lies closest in $\vec{p}_\perp$ and use only those jets for reconstructing the presumed $\tilde{\chi}_1^0$ CM's. The combinatorics are thus brought down to very low levels. One technicality involved is how we deal with situations

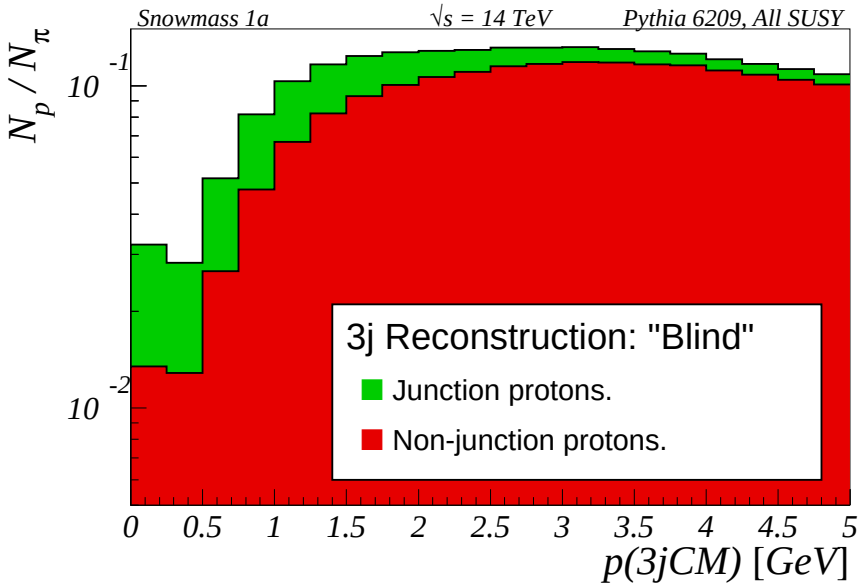

Figure 24: Reconstructed proton momentum spectrum in the 3-jet CM frame for the "blind" neutralino decay jet identification.

where one jet turns out to be the closest in $\vec{p}_\perp$ to more than one of the neutralino daughters. This situation can arise for instance if those two daughters were sufficiently close together to be clustered to a single jet, or if one of the daughters produced a jet that lies outside the active calorimetry range. Such systems are not included in the analysis.

For each accepted 3-jet system we search for candidate junction protons and charged pions in exactly the same manner as for the blind analysis. Only 1% of the junction protons within the detector acceptance survive, still with a contamination of about 0.2% of the non-junction protons, but the junction proton distribution is now more sharply peaked towards low momenta (in the 3-jet CM frame) and the non-junction protons are found at higher momenta.

The distribution of proton to pion ratios as a function of p in the 3-jet system CM frame is shown in Fig. 25. A noticeable improvement of the ratio of junction protons to non-junction protons can be seen in the region below $\sim$ 1 GeV. For the blind analysis, cf. Fig. 24, this ratio was about 2. The corresponding number for Fig. 25 is closer to 4, approximately the same factor as for the isolated neutralino decay, Fig. 18.

We thus conclude that even with all the surrounding activity in fully generated pp collisions, it *is* possible, with a good jet selection, to arrive at a proton sample of almost the same purity as for the case of isolated decay. It should be remembered, though, that we are not here talking about an *excess* of protons of a factor of 4, since the division into junction baryons and non-junction baryons is not an experimental observable. What is expected from ordinary $q\overline{q}$ fragmentation is represented in Fig. 18 by circles and crosshairs, and we see that relative to *this* number, the excess is only about a factor 1.5. We note that one does not have to rely on a Monte Carlo estimate of the proton to pion ratio. A study of reference background samples, of multijet events in configurations not significantly contaminated by SUSY events, will allow an absolute determination of the proton fraction from data. We therefore believe that even such a modest difference as a 50% enrichment should be clearly visible, given enough statistics.

Note that the rate of baryon production in high-energy collisions offers one puzzling

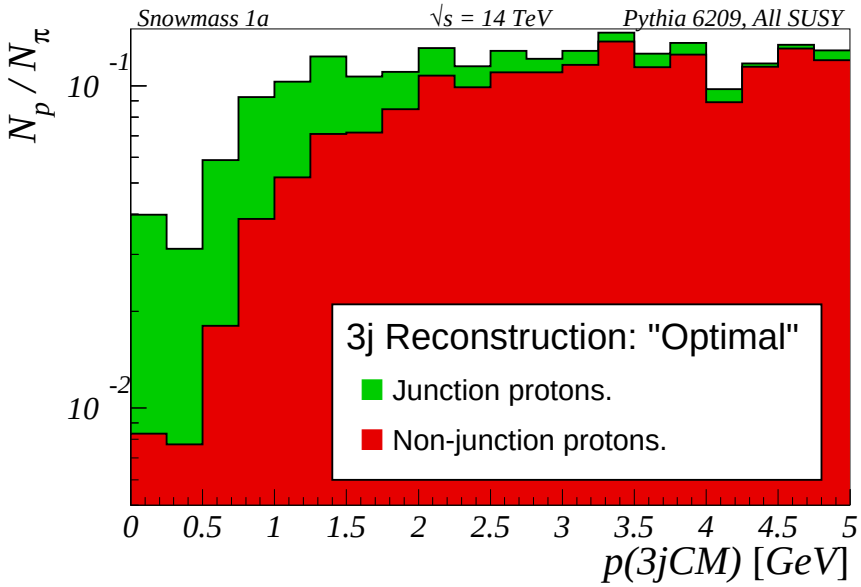

Figure 25: Reconstructed proton spectrum in the 3-jet CM frame for the "optimized" neutralino decay jet identification.

outstanding problem in our understanding of QCD: why are fewer kaons and protons produced in ep/γp events than in e^+e^- ones? This problem has been with us since several years [42], and has been reconfirmed by recent HERA studies [43]. One possible explanation is the 'quiet string scenario' [42], namely that soft gluon emission around the perturbative–nonperturbative border is less profuse in ep/γp events, where only part of the event feels a hard scale, than in e^+e^- ones, where the whole event derives from a hard-scale process. The string would then be less 'wrinkled' in the former case than the latter, thus have a smaller effective string tension, and thereby a lesser production of heavier particles. This is very speculative, however, and having to give up jet universality would be uncomfortable, to say the least. One possible test in Deeply Inelastic Scattering would be a comparison of the current hemisphere in the Breit frame with the rest of the event. It is also unknown whether Tevatron collider events more resemble LEP or HERA ones in this respect. In the quiet string scenario, one would expect particles associated with the perturbative jets, i.e. the particles we have studied, to resemble LEP, while the underlying event again could be quieter and therefore also contain fewer baryons. The older UA5 measurements on K^0_S [44] do not indicate any problem for the standard string model [32]. Hopefully the issue will be settled well before a study of observed potential BNV events is initiated.

6.3 BNV two-body decays

We now follow up the discussion in subsection 5.5, considering the process $e^+e^- \to \tilde{t}_1(\to \bar{d}\bar{s})\tilde{t}_1^*(\to ds)$ for a linear collider, TESLA or the NLC/JLC, using the mSUGRA parameters of Snowmass point 5 to represent a generic "light stop" scenario. Although the 220 GeV stop mass of this benchmark point is small enough to allow pair-production at 500 GeV, the amount of junction–junction annihilation depends strongly on the stop boost, meaning that essentially no junctions would survive at CM energies close to threshold in our preferred stringlength-minimization scenario. Thus, to increase the 2-junction rate, and

also to get a higher total production cross section, we are lead to consider an 800 GeV option. Note that if the BNV couplings are small, we expect string breaks between the stops to occur *before* decay. Such breaks would sever the connection in colour space between the two junctions and thus effectively eliminate the possibility of obtaining 0-junction topologies.

At the chosen CM energy, the stop boost $\gamma_{\tilde{t}} = E_{\tilde{t}}/m_{\tilde{t}} = E_{\rm CM}/2m_{\tilde{t}} \sim 1.8$, making us expect that, in the case of large BNV couplings, about 40% of the junction–junction systems survive to give rise to junction baryons, cf. Fig. 8. The remaining 60% of the events presumably represent a more or less irreducible background to our search, since they contain no signal (junction) baryons and only differ from the signal events at the hadronization level, cf. Fig. 22 and the discussion there. Of course, once BNV is established, also the rate of junction annihilation by itself could offer interesting information on QCD.

Similarly to the LHC study, we assume that a clean sample of $\tilde{t}_1\tilde{t}_1^*$ events has been isolated, so that SM as well SUSY backgrounds can be neglected. A further simplification we make is to disregard the effects of brems- and beam-strahlung in the initial state, mostly since the latter depends sensitively on the beam parameters and we do not wish to become too machine-specific at this stage.

So as not to be completely unrealistic in regard to detector acceptance, we ignore all particles closer than 5° to the beam pipe and reconstruct only charged particles which have $p_\perp > 0.5$ GeV. Beyond these crude cuts, no effort is made to simulate detector effects. For jet reconstruction we use Durham $y_{\rm D} = 10^{-2.5} \approx 0.003$. This results in about 65% 4-jet events, 20% 5-jets, and 10% 3-jets for the process considered. Naturally, the events with more than 4 jets are those which involve emissions of hard gluons. This means partly that we are facing a larger combinatorics, and partly that we are less certain in which direction the junctions went and hence in which direction to look for the junction protons. For the 3-jet events, two of the original four jets have ended up very close to each other. With a smaller $y_{\rm D}$ those jets might be resolved, but it is not clear that much could be gained by this. Thus, all but the 4-jet events are removed from the further analysis.

We begin by simply performing a proton-count within the detector acceptance, normalizing to the charged pion multiplicity, as we did for the LHC study. The result, shown in Fig. 26, is markedly better than for the LHC case, Fig. 23, chiefly due to the cleaner environment and that we now go down to $p_\perp = 0.5$ GeV. Even though, in Fig. 26a, we have only a 40% rate of 2-junction configurations, about 30% of the protons below 1.5 GeV are junction protons. This should be compared with Fig. 26b, where we have turned off junction–junction annihilation.

Fortunately, it is again possible to purify the sample somewhat more. First, we identify which of the 3 possible pair-by-pair combinations of the four jets is most consistent with both pairs having the invariant mass of the $\tilde{t}_1$, by selecting the configuration with the smallest value of $\Delta M \equiv |m_{ij} - m_{\tilde{t}_1}| + |m_{kl} - m_{\tilde{t}_1}|$.

The mass distributions of the pairs thus selected are shown in Fig. 27 for dynamically mixed (default) 2-junction and 0-junction topologies (solid curve), for 2-junction topologies in all events (dotted curve), and for 0-junction topologies in all events (dot-dashed curve). As before, note that the latter sample has a small contamination of 2-junction events, from perturbative breakups in the $\tilde{t}_1\tilde{t}_1^*$ shower. All the distributions are shifted a few GeV towards larger masses, relative to the nominal $\tilde{t}_1$ mass, but the 0-junction topologies are shifted a bit more and have a wider distribution compared to the 2-junction ones. The shift of the peaks is due to a string effect: the fact that either one junction–junction string or two $q\overline{q}$ strings are spanning the range *between* the two jet systems increases the

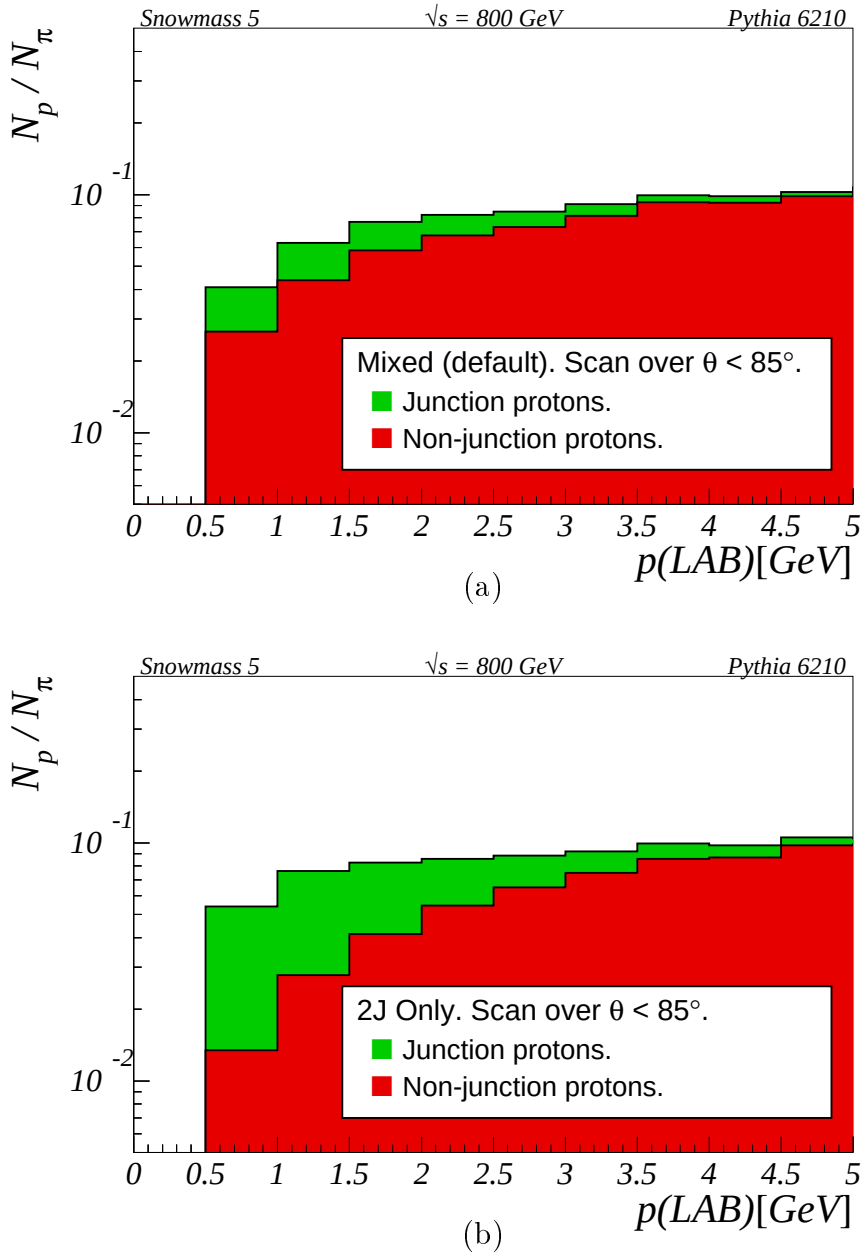

Figure 26: Reconstructed momentum spectrum for the ratio of protons to charged pions in a simple scan over the detector volume: (a) mixed 2-junction and 0-junction topologies and (b) pure 2-junction topologies.

hadronic multiplicity in this region. In the former topology, all the hadrons produced in a junction–junction string add mass to whichever stop they are clustered with. (The energy of these hadrons is taken from the kinetic energy of the stops, which are slowed down correspondingly.) In the latter topology, the two separately hadronizing $q\overline{q}$ systems produce even more extra soft particles in between the $\tilde{t}_1$ and $\tilde{t}_1^*$ jets. Also note that this skews the reconstructed jet directions away from the original parton directions, towards larger opening angles, which is an alternative way of expressing that the jet–jet pairs end up having invariant masses slightly above the actual resonance mass. In events with multiple gluon emissions in the $\tilde{t}_1\tilde{t}_1^*$ system — few to begin with and further reduced by our cuts — the zig-zag pattern illustrated in Fig. 7b further tends to favour large string lengths

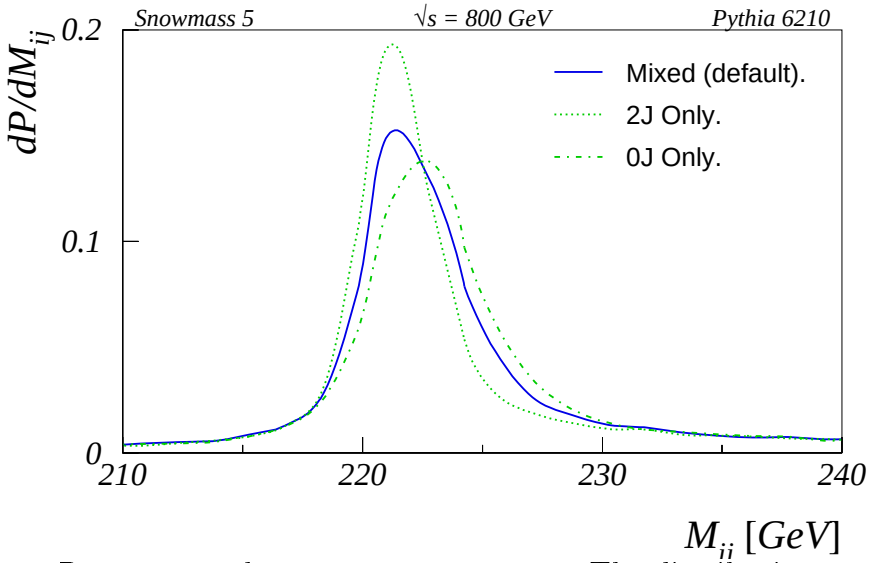

Figure 27: Reconstructed jet–jet mass spectrum. The distributions are normalized so as to integrate to the 4-jet rates.

and thereby large mass shifts in the 0-junction configuration. It is important to remember that the bulk of the particle production is associated with the four (anti)quark jet directions, however, and what we discuss here are smaller perturbations on this picture.

To summarize, we do not expect that a double peak, one from the 2-junction topologies and another from the 0-junction ones, will be visible in the jet–jet mass spectrum, but we do expect a small enrichment of 2-junction topologies on the low side of the peak relative to the high side of it. Therefore we impose a slightly asymmetric cut on the jet–jet masses, $m_{\tilde{t}_1} - 10 \text{ GeV} < M_{ij} < m_{\tilde{t}_1} + 5 \text{ GeV}$. Note that both jet–jet pairs in an event are required to pass this cut, or the event is rejected, this mainly to ensure that both sides of the event are well reconstructed.

Having thus reduced the combinatorics, it is a matter of simple kinematics to show that the two daughters from each stop decay will be separated by more than 60° at the 800 GeV CM energy. Adding parton showers and hadronization effects will not change this limit appreciably, and so we place a cut requiring jet pair opening angles larger than 60°. Larger opening angles, from asymmetric decays and/or slowed-down stops, tend to favour the 0-junction topologies, i.e. give less signal. Therefore, and since we aim to look for junction protons *between* the two daughter jets, we require a maximal jet–jet opening angle of 120°.

For the remaining jet–jet pairs, we may now safely presume that the junction baryon, if there is one, is predominantly travelling in roughly the same direction as the stop did, in between the two daughter jets. To measure how much "in between" two jets a particle is, we construct

$$\hat{\theta}_{\mathrm{pj_1j_2}} = \frac{1}{\sqrt{2}} \sqrt{\left(\frac{2\theta_{\mathrm{pj_1}}}{\theta_{\mathrm{j_1j_2}}} - 1\right)^2 + \left(\frac{2\theta_{\mathrm{pj_2}}}{\theta_{\mathrm{j_1j_2}}} - 1\right)^2}, \tag{26}$$

where θ_{pj_i} is the angle between jet i and the particle in question, and $\theta_{\mathrm{j_1j_2}}$ is the inter-jet angle. The measure is constructed so as to have the value $\hat{\theta} = 0$ when a particle is lying exactly between the two jets and $\hat{\theta} = 1$ when a particle is exactly aligned with one or the other of the jet directions. Note that $\theta_{\mathrm{pj_1}} + \theta_{\mathrm{pj_1}} \geq \theta_{\mathrm{j_1j_2}}$, where the equality holds for particles lying between the two jets and in the plane defined by the jet directions.

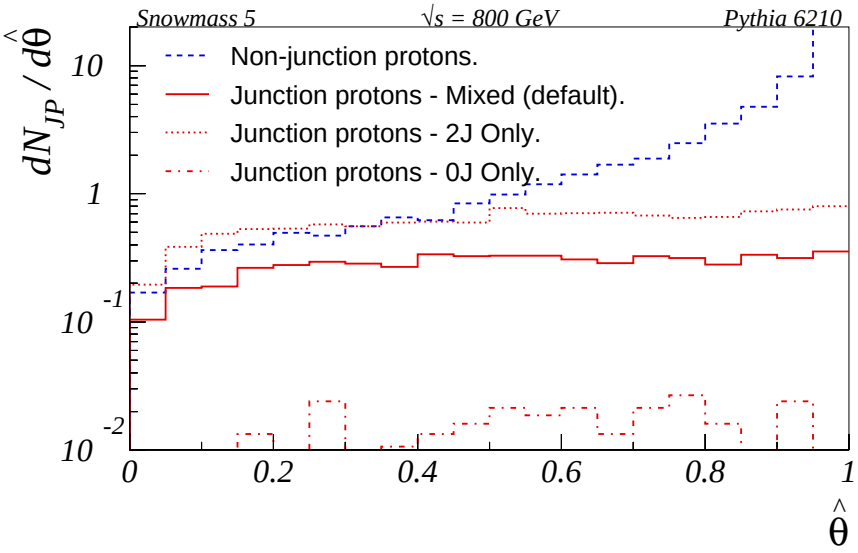

Figure 28: Distributions in $\hat{\theta}_{\mathrm{pj_1j_2}}$ of junction protons for dynamically mixed (default) 2-junction and 0-junction topologies (solid lines), 2-junction only (dotted lines), and 0-junction only (dash-dotted lines). The dashed histogram represents the non-junction protons. These are only shown for the default case, the non-default spectra being very similar.

In Fig. 28 we show the distributions of junction protons and ordinary protons in this variable for events passing the previous cuts. Note that the junction proton distributions, even for the pure 2-junction topologies, do not integrate to 2 over the $\hat{\theta}$ range shown on the plot. This owes to the simple facts that many junction protons are irretrievably lost by the $p_\perp \geq 0.5$ GeV cut we imposed above and that a non-vanishing fraction of them have $\hat{\theta}_{\mathrm{pj_1j_2}} > 1$. The logarithmic scale on the plot is called for by the very strong peaking of the non-junction proton spectrum towards the jet axes. We observe that the shape of the junction proton spectrum is rather flat, independently of whether we allow junction–junction annihilation or not, although the normalization of course changes. When junction–junction annihilation is forced (dot-dashed curve), only those junctions which are separated by $\mathrm{g} \to \mathrm{q\overline{q}}$ splittings in the cascades of the $\tilde{\mathrm{t}}_1\tilde{\mathrm{t}}_1^*$ system survive after hadronization, hence extremely few junction protons are produced. We impose a cut requiring $\hat{\theta}_{\mathrm{pj_ij_j}} < 0.5$, thereby cleaning out most of the jet-associated protons.

Furthermore, we may use the fact that the junction proton momentum spectrum is most strongly peaked in the junction rest frame (JRF), cf. Fig. 17. Analogously to what we did for the LHC study, we therefore construct an approximate JRF for each jet pair, in each case using the linear combination of the momenta of the opposing pair as the "third leg". Including the above-mentioned cuts, this results in the multiplicity distribution Fig. 29a, now with about 60% of the protons below 1 GeV being junction protons. A rough estimate is that this corresponds to about 50 junction protons per 100 fb^{-1} of integrated luminosity. With junction–junction annihilation turned off, the distribution changes to that of Fig. 29b, with about 80% of the protons below 1 GeV being junction protons, corresponding to more than 100 junction protons per 100 fb^{-1}.

Thus, for the process and SUSY scenario considered here, small BNV couplings substantially increase the possibility of directly detecting the extra (anti)baryons.

Going further and establishing the absolute rate of junction protons per $\tilde{\mathrm{t}}_1\tilde{\mathrm{t}}_1^*$ event, with the BNV branching fractions known, would obviously amount to a direct measurement of

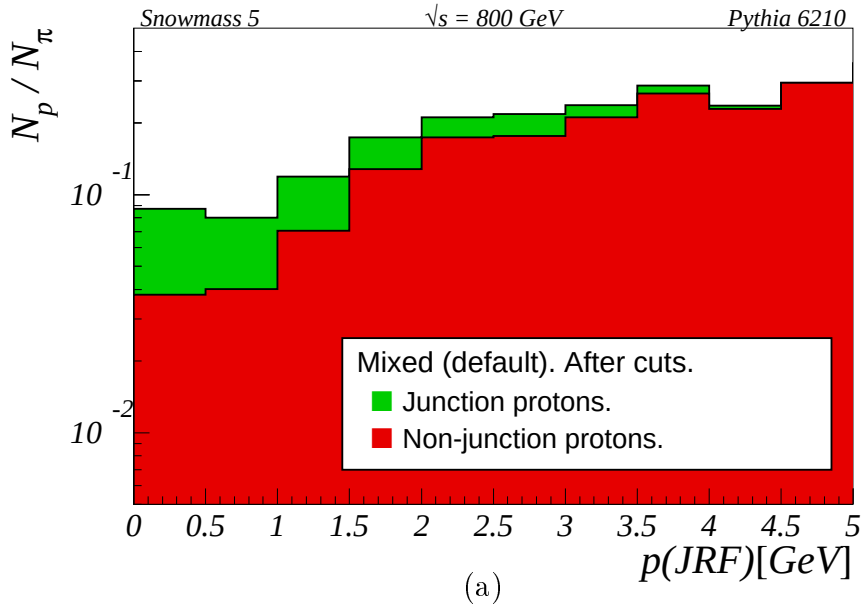

(a)

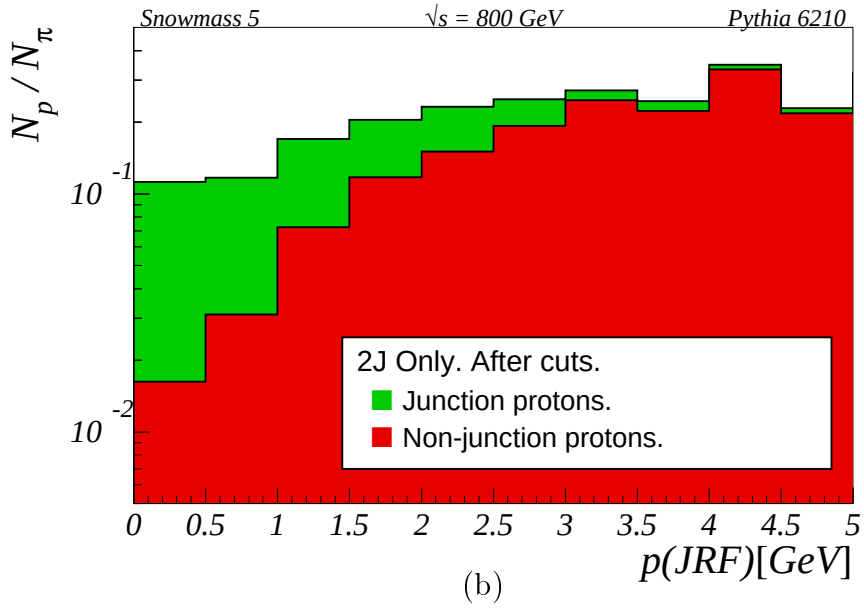

(b)

Figure 29: Reconstructed momentum spectrum in the approximated junction rest frame for the ratio of protons to charged pions: (a) dynamically mixed (default) 2-junction and 0-junction topologies and (b) 2-junction topologies only.

the junction–junction annhilation rate. Such a measurement would be interesting from a QCD perspective, since it enables us to confront the value predicted by our model with an experimental result. We therefore here also briefly discuss an alternative way of measuring this quantity.

In the 0-junction topology, with at least two strings spanning the rapidity region between the stops, we here expect a higher average multiplicity than for the 2-junction case, in which only one string spans this region. Naïvely then, the charged multiplicity between the two jet pairs should be at least twice as large for 0-junction topologies as compared to 2-junction ones. However, this drastically oversimplifies the true situation.

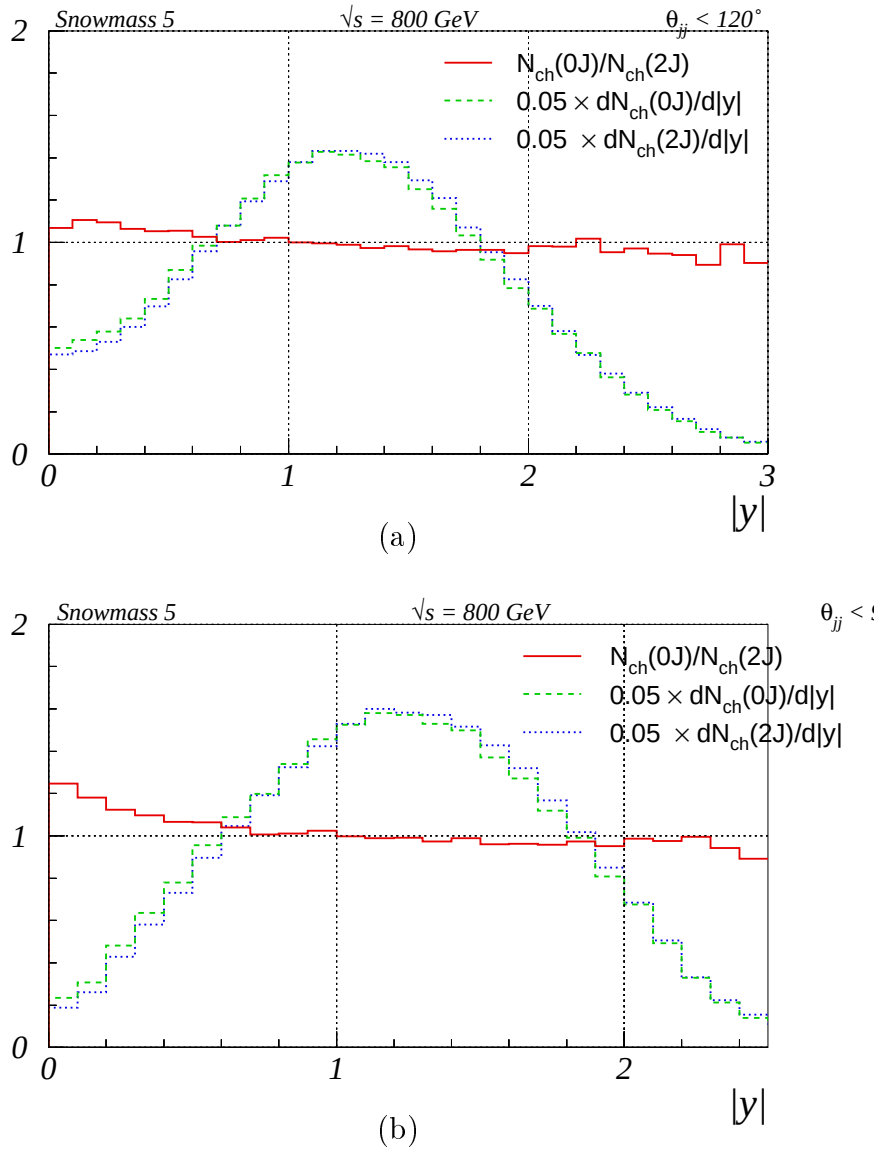

Figure 30: Charged multiplicities of 0-junction topologies (dashed lines) and 2-junction topologies (dotted lines) as functions of rapidity along the stop-antistop thrust axis for (a) $\theta_{\rm jj} \leq 120^\circ$ and (b) $\theta_{\rm jj} \leq 90^\circ$ (all other cuts are as for the junction proton search). The ratios of the distributions are shown with solid lines.

Asymmetric decays of the stops and the addition of parton showers will in general smear the difference to a much lower factor, to the point where it becomes questionable whether this method is at all feasible. To investigate, we select events passing the above-mentioned cuts and plot the charged multiplicity as a function of the absolute value of the rapidity with respect to the stop–antistop momentum axis. The resulting rapidity distributions, shown in Fig. 30a, only exhibit a negligible increase in the ratio $(\mathrm{d}N_{0\mathrm{J}}/\mathrm{d}|y|)/(\mathrm{d}N_{2\mathrm{J}}/\mathrm{d}|y|)$ in the region $|y| \sim 0$.

One reason for this is that the central region is not free from jet activity. Specifically, if the decay products of one of the stops are aligned with the original direction of motion of the stop, the backward jet will end up in the "wrong hemisphere". The most extreme of these cases are already removed by the requirement of jet–jet opening angles

smaller than 120°, as was imposed above, but this cut still leaves room for jet activity in the mid-rapidity region. To clean out the worst of this contamination, in Fig. 30b, we have tightened the cut on maximal jet–jet opening angles to $\theta_{\rm jj} \leq 90°$. One notices that the average multiplicity in the central region drops, and that the ratio between the multiplicities in the two topologies increases in this region. Ultimately, to get as little contamination from jet tails as possible in the central region, one should go as close as possible to the kinematic limit, $\theta_{\rm jj} = 60°$, where the rapiditity of all jets, with respect to the stop-antistop momentum axis, is $|y| \sim 1.3$. The necessary compromise thus lies between minimizing the jet contamination in the central region and obtaining sufficient statistics. For the present, we merely note that the central multiplicity *is* sensitive to the choice of string topology but that it will presumably be hard to use it for a precise determination of the junction–junction annihilation rate.

7 Summary

The physics scenario studied here may not be the most likely one. First we have to accept supersymmetry, then that R-parity is violated, and finally that it is baryon rather than lepton number that is affected. Nevertheless, it is one possibility among many that should be considered in studies of the high-energy frontier, and one that has maybe received less attention than others of equal likelihood to be correct.

In particular, it is important to know whether such a scenario introduces new special demands on detectors. Obviously the whole normal artillery of jet reconstruction and mass peaks need to be brought to bear on the issue, in order to find a signal for new physics. This may already be enough to favour some specific scenarios, such as BNV SUSY. However, given that the unique aspect of BNV is the creation of an additional baryon or antibaryon, a discovery of BNV SUSY would not be complete without a clear signal that indeed baryon number is violated.

Since baryons are produced also in normal hadronization processes, it will not be feasible to associate one specific baryon uniquely with the BNV process, but only to establish an excess of baryon production. This excess will not be large enough to help us, unless we know where to look, and thereby can reduce the background noise level.

The string junction model we develop in this article offers us the tools to do precisely that. The string concept itself is the most successful approach we have to the description of hadronization at high energies. The junction concept is also well-established in the literature, to describe baryon colour topologies and confinement aspects. It has never before (to the best of our knowledge) been developed and implemented into a realistic hadronization framework, however.

Armed with this detailed model, we can predict where the baryon excess should be found. In general, the junction baryon will have low momentum in the rest frame of the process that generates the BNV. For the specific case of neutralino or chargino BNV decay at LHC, we show how this translates into explicit predictions. Typically we need to impose some cut like $p_\perp > 1$ GeV to get away from the bulk of the underlying event activity, but beyond that the main demand is for a good $\mathrm{p}/\overline{\mathrm{p}}$ identification at rather low momenta, i.e. a few GeV. Failing this, at least Λ tagging should be well developed.

We believe this to be the first example where non-QCD physics interests put precise demands on baryon identification. Thereby it offers an interesting test case for further detector performance studies. The specific distributions we show for LHC are only intended to "whet the appetite", and are in no way blueprints for a realistic analysis. Background

studies will be essential, not only in the search of a signal, but also to help calibrate the normal rate of baryon production. Especially disconcerting is here the experimental indications of a difference in the baryon fraction between different kinds of events, e.g. ep vs. e^+e^-.

Studies could also be performed for other machines. Unfortunately, it is doubtful whether the Tevatron could produce enough BNV events to allow an analysis along the lines we have in mind, given that no signs of SUSY have been seen so far. In contrast, BNV neutralino or chargino decays at a future linear e^+e^- collider should be much cleaner and thereby simpler to analyse — one reason we have not considered it here. The difficult questions at such a collider could rather come in the analysis of BNV $\tilde{t}\tilde{t}^*$ events, where the threshold region production would allow two different event topologies, one with an extra baryon–antibaryon pair and one without. We find that the relative importance of these topologies may not be easy to pin down experimentally.

It can be questioned how unique the proposed junction hadronization framework is, given that it is not based on any experimental tests to existing data. On the technical level, certainly a number of approximations and simplifications have been introduced, but we have demonstrated that the resulting uncertainties appear under control. More serious is the issue whether the whole ansatz as such is what happens in Nature, and here no guarantees can be given. What can be said its that there is currently no alternative approach that looks anywhere near as credible.

One specific example is here offered by Herwig. This generator maps a three-quark cluster onto a quark–diquark one, which then is fragmented along a single axis. Since the baryon cluster mass typically is very large — in part a consequence of a low shower activity in these events — the fragmentation can deform the event appreciably and, more significantly, kick the baryon out to surprisingly large momenta.

That is not to say there is no room for improvement in our Pythia implementation. We did not (yet) include the matrix-element information to give non-isotropic three-body BNV decays, the BNV production processes are not implemented at all, and our shower description is not as sophisticated as e.g. for $Z^0 \to q\overline{q}$ decays. Such imperfections could influence estimates of the experimental acceptance rate of BNV decays. Given all the other uncertainties at this stage of the game, one should not exaggerate their importance, however. Once SUSY is observed, with indications of BNV, further work would be reasonable.

The development of a model for the hadronization of junction string topologies is not only relevant for BNV SUSY. In principle we would assume the same topology for the incoming baryons in high-energy pp or $p\overline{p}$ collisions. So long as only one valence quark is kicked out of a proton, the two remaining quarks drag the junction along and thereby form an effective diquark. But in multiple interaction approaches there is every possibility for two quarks to be kicked out, in different directions, and with colours rearranged in the process. Thereby the baryon number can start to drift in the event. This scenario was advertised in [32], but has not been studied further till now. The recent increased interest in semihard physics at hadron colliders [45], which has confirmed the basic validity of the Pythia framework but also pointed at problems, here provides a stimulus for further developments. Hopefully, refined models could allow us to understand the excess of baryon number observed in the central region of events in a number of experiments ([46] is a far from complete list). Here junction scenarios have already been proposed as a possible mechanism [47], but without any solid modelling efforts.

A reason for us to begin with the SUSY BNV studies, rather than with pure QCD ones, is that the latter inevitably will come to involve further uncertainties, such as the

details of the multiple interactions scenario. Nevertheless, the hope is that continued QCD-related studies may add support for the validity of the junction scenario proposed in this article. Thereby the physics of junction fragmentation offers a prime example of a topic where the exploration of very conventional and very unconventional physics goes hand in hand.

Acknowledgements

The authors would like to thank Gösta Gustafson for helpful discussions on the string length of junction topologies, and Frank Paige and Albert de Roeck for useful information on the ATLAS and CMS proton identification capabilities. We are also grateful to the NorduGrid project, for inviting us to test their facilities. Many of our results were obtained with grid computing.

References

[1] I. Hinchliffe and T. A. Kaeding, Phys. Rev. D **54** (1996) 914.

[2] H. Baer, F.E. Paige, S.D. Protopopescu and X. Tata, hep-ph/0001086.

[3] G. Corcella, I.G. Knowles, G. Marchesini, S. Moretti, K. Odagiri, P. Richardson, M.H. Seymour and B.R. Webber, JHEP **0101** (2001) 010

[4] S. Katsanevas and P. Morawitz, Comput. Phys. Commun. **112** (1998) 227.

[5] T. Sjöstrand, P. Edén, C. Friberg, L. Lönnblad, G. Miu, S. Mrenna and E. Norrbin, Computer Phys. Commun. **135** (2001) 238;
T. Sjöstrand, L. Lönnblad and S. Mrenna, LU TP 01-21 [hep-ph/0108264].

[6] P.Z. Skands, Cand. Scient. thesis, Copenhagen University (2001), hep-ph/0108207.

[7] P.Z. Skands, Eur. Phys. J. **C23** (2002) 173.

[8] H.K. Dreiner, P. Richardson and M.H. Seymour, JHEP **0004** (2000) 008.

[9] S. Moretti, K. Odagiri, P. Richardson, M.H. Seymour and B.R. Webber, JHEP **0204** (2002) 028.

[10] B.C. Allanach, A.J. Barr, L. Drage, C.G. Lester, D. Morgan, M.A. Parker, B.R. Webber and P. Richardson, JHEP **0103** (2001) 0248;
B.C. Allanach, A.J. Barr, M.A. Parker, P. Richardson and B.R. Webber, JHEP **0109** (2001) 021.

[11] P. Z. Skands, to appear in the proceedings of SUSY02, Hamburg, Germany, 17-23 Jun 2002, LU TP 02-35 [hep-ph/0209199].

[12] X. Tata, Lectures presented at the IX JAS Summer School, hep-ph/9706307.

[13] S. Dimopoulos et al., Phys. Rev. D **41** (1990) 2099;
R. J. Oakes et al., Phys. Rev. D **57** (1998) 534;
B. Allanach et al., contributed to 'Physics at Run II: Workshop on Supersymmetry/Higgs' (1998), hep-ph/9906224;
E. L. Berger, B. W. Harris and Z. Sullivan, Phys. Rev. D **63** (2001) 115001.

[14] L. Lönnblad, Computer Phys. Commun. **71** (1992) 15.

[15] I.G. Knowles et al., in 'Physics at LEP2', eds. G. Altarell, T. Sjöstrand and F. Zwirner, CERN 96–01, Vol. 2, p. 103;
P. Bambade et al., in 'Reports of the Working Groups on Precision Calculations for LEP2 Physics', eds. S. Jadach, G. Passarino and R. Pittau, CERN 2000–009, p. 137.

[16] M.H. Seymour, Computer Phys. Commun. **90** (1995) 95.

[17] G. Corcella and M.H. Seymour, Phys. Lett. **B442** (1998) 417.

[18] M. Bengtsson and T. Sjöstrand, Phys. Lett. **B185** (1987) 435; Nucl. Phys. **B289** (1987) 810

[19] E. Norrbin and T. Sjöstrand, Nucl. Phys. **B603** (2001) 297.

[20] V.A. Khoze, L.H. Orr and W.J. Stirling, Nucl. Phys. **B378** (1992) 413.

[21] B. Andersson, G. Gustafson, G. Ingelman and T. Sjöstrand, Phys. Rep. **97** (1983) 31;
B. Andersson, 'The Lund Model' (Cambridge University Press, 1998).

[22] R.K. Ellis, W.J. Stirling and B.R. Webber, 'QCD and Collider Physics' (Cambridge University Press, 1996), and references therein.

[23] B. Andersson, G. Gustafson and T. Sjöstrand, Nucl. Phys. **B197** (1982) 45.

[24] B. Andersson, G. Gustafson and T. Sjöstrand, Physica Scripta **32** (1985) 574;
P. Edén and G. Gustafson, Z. Phys. **C75** (1997) 41.

[25] I.G. Knowles and G.D. Lafferty, J. Phys. **G23** (1997) 731, and references therein.

[26] T. Sjöstrand, Nucl. Phys. **B248** (1984) 469.

[27] X. Artru, Nucl. Phys. **B85** (1975) 442.

[28] M. Imachi, S. Otsuki and F. Toyoda, Progr. Theor. Phys. **54** (1975) 280;
Y. Igarashi et al., Progr. Theor. Phys. Suppl. **63** (1978) 49;
G.C. Rossi and G. Veneziano, Nucl. Phys. **B123** (1977) 507.

[29] L. Montanet, G.C. Rossi and G. Veneziano, Phys. Rep. **63** (1980) 149.

[30] G. 't Hooft, Physica Scripta **25** (1982) 133.

[31] B. Andersson, G. Gustafson, I. Holgersson and O. Månsson, Nucl. Phys. **B178** (1981) 242.

[32] T. Sjöstrand and M. van Zijl, Phys. Rev. **D36** (1987) 2019.

[33] I. Montvay, Phys. Lett. **84B** (1979) 331.

[34] V.A. Khoze and T. Sjöstrand, Phys. Lett. **B328** (1994) 466.

[35] B. Andersson, G. Gustafson and B. Söderberg, Z. Phys. **C20** (1983) 317;
B. Andersson, S. Mohanty and F. Söderberg, Nucl. Phys. **B646** (2002) 102.

[36] B. C. Allanach et al., in 'Proc. of the APS/DPF/DPB Summer Study on the Future of Particle Physics' (Snowmass 2001), eds. R. Davidson and C. Quigg [hep-ph/0202233].

[37] S. Catani, Yu.L. Dokshitzer, M. Olsson, G. Turnock and B.R. Webber, Phys. Lett. **B269** (1991) 432.

[38] S. Moretti, L. Lönnblad and T. Sjöstrand, JHEP **9808** (1998) 001.

[39] R.K. Ellis, D.A. Ross, and A.E. Terrano, Nucl. Phys. **B148** (1981) 421.

[40] ATLAS Collaboration, Technical Report, CERN/LHCC 99-14.

[41] Particle Data Group, K. Hagiwara et al., Phys. Rev. **D66** (2002) 010001.

[42] T. Sjöstrand, J. Phys. **G22** (1996) 709, and references therein.

[43] H1 Collaboration, abstract 1002, submitted to ICHEP02, Amsterdam, The Netherlands, 24–31 July 2002.

[44] UA5 Collaboration, G.J. Alner et al., Nucl. Phys. **B258** (1985) 505.

[45] CDF Collaboration, D. Acosta et al., Phys. Rev. **D65** (2002) 072005;
CDF Collaboration, T. Affolder et al., Phys. Rev. **D65** (2002) 092002;
D0 Collaboration, V.M. Abazov et al., hep-ex/0207046;
R.D. Field and A. Kharchilava, presentations at the 'Matrix Element and Monte Carlo Tuning Workshop', Fermilab, October 4, 2002,
`http://www-cpd.fnal.gov/MCTuning/`.

[46] G. Belletini et al., Nuovo Cimento **A42** (1977) 85;
B. Alper et al., Nucl. Phys. **B100** (1975) 237;
A. Breakstone et al., Z. Physik **C28** (1985) 335;
H1 Collaboration, paper 556, submitted to ICHEP98, Vancouver, July 1998, and in preparation;
STAR Collaboration, C. Adler et al., Phys. Rev. Lett. **86** (2001) 4778;
PHENIX Collaboration, K. Adcox et al., Phys. Rev. Lett. **89** (2002) 092302;
PHOBOS Collaboration, B.B. Back et al., nucl-ex/0206012;
BRAHMS Collaboration, I.G. Bearden et al., nucl-ex/0207006.

[47] D. Kharzeev, Phys. Lett. **B378** (1996) 238;
B. Kopeliovich and B. Povh, Z. Physik **C75** (1997) 693;
S.E. Vance, M. Gyulassy and X.-N. Wang, Phys. Lett. **B443** (1998) 45;
G.T. Garvey, B.Z. Kopeliovich, B. Povh, Comments Mod. Phys. **A2** (2001) 47.